Zinc oxide (ZnO) nanostructures were synthesized by hydrothermal method. This technique has many preferable properties such as low cost, low power request, simple apparatus, and safety for environment with high quality products. The hydrothermal system consist of two mainly parts electrical controller and reaction chamber, all parts are maddened home with global specifications. ZnO (1g) nanoparticles and Sodium Hydroxide (NaOH) with concentrations 3M, 6M were the starting materials for the chemical reaction under stirring. The suspension was transferred into a Teflon lined sealed stainless steel autoclave and kept at 70 o C and 90 o C separately for reaction time 24, 48 and 72 hour. ZnO nano structures were successfully synthesized using the concentrations (3M, 6M) of NaOH prepared by hydrothermal method, which provided us with a variety in structure (Nanotubes, nanorods, Nanobelts, nanosticks, lettuce leaf, flowers-like, and heterogeneous structures).

Thamir A.A. Hassan: Ph.D./Group of Nanotechnology and Materials/Physics Department/College of Science/University of Baghdad. Now he is President of Al-Karkh University of Science/Ministry of Higher Education and Scientific Research. Has 6 patents, 20 Conf. Contribution and 13 Publications. U.S. Excellence Award. Member of ISS, ASME. Editor in IJNN.

978-3-659-92756-0

Synthesis with Hydrothermal Method

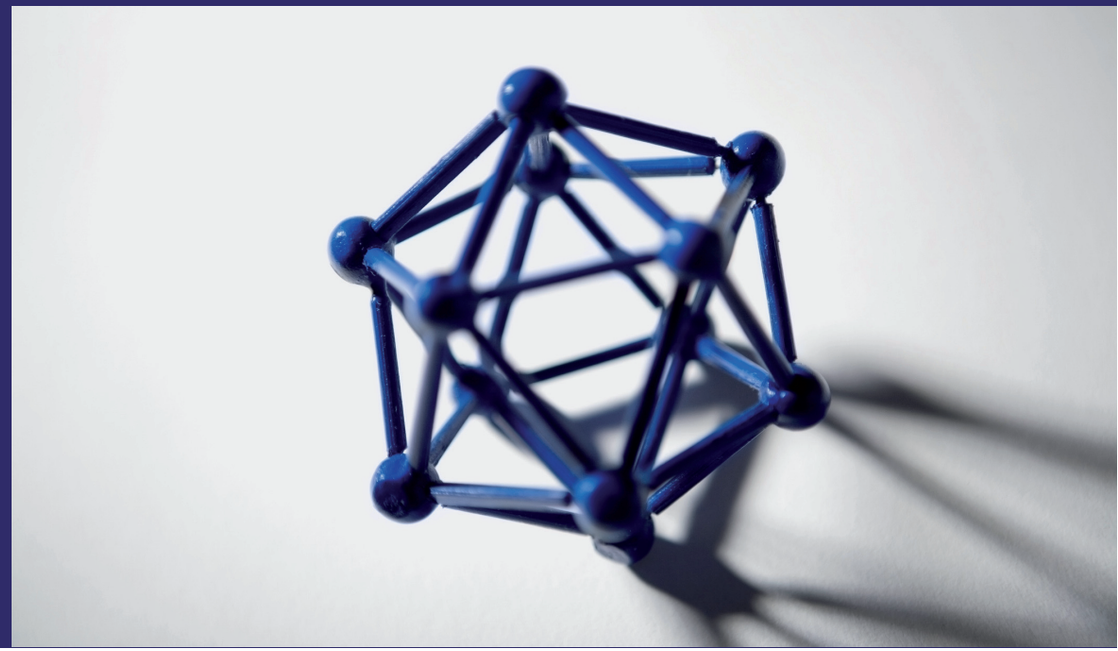

Thamir A.A. Hassan
Ali Q. Tuama

Nanostructures Zinc Oxide (ZnO) Synthesis with Hydrothermal Method

A.A. Hassan, Q. Tuama

LAP LAMBERT Academic Publishing

Thamir A.A. Hassan
Ali Q. Tuama

Nanostructures Zinc Oxide (ZnO) Synthesis with Hydrothermal Method

Thamir A.A. Hassan
Ali Q. Tuama

Nanostructures Zinc Oxide (ZnO) Synthesis with Hydrothermal Method

LAP LAMBERT Academic Publishing

Impressum / Imprint
Bibliografische Information der Deutschen Nationalbibliothek: Die Deutsche Nationalbibliothek verzeichnet diese Publikation in der Deutschen Nationalbibliografie; detaillierte bibliografische Daten sind im Internet über http://dnb.d-nb.de abrufbar.

Bibliographic information published by the Deutsche Nationalbibliothek: The Deutsche Nationalbibliothek lists this publication in the Deutsche Nationalbibliografie; detailed bibliographic data are available in the Internet at http://dnb.d-nb.de.

Coverbild / Cover image: www.ingimage.com

Verlag / Publisher:
LAP LAMBERT Academic Publishing
ist ein Imprint der / is a trademark of
OmniScriptum GmbH & Co. KG
Bahnhofstraße 28, 66111 Saarbrücken, Deutschland / Germany
Email: info@omniscriptum.com

Herstellung: siehe letzte Seite /
Printed at: see last page
ISBN: 978-3-659-92756-0

Nanostructures Zinc Oxide (ZnO) Synthesis with Hydrothermal Method

By

Thamir A.A. Hassan
Ali Q. Tuama

To Dedication

To the blood of the martyrs of Iraq
To Champions Iraq on the battlefield
To Champions the holy popular crowd

Authors

Acknowledgments

First, we should like to express my deep thanks to the Almighty God, ALLAH JALA JALALAH, for what we have achieved.

We would like to express our deep gratitude and appreciation to ***Dr.Abdulkareem M. Ali*** at Chemical Dept .as well as ***Eng. Isam Al-Radhi Abbas*** .

PREFACE

Zinc oxide (ZnO) nanostructures were synthesized by hydrothermal method. This technique has many preferable properties such as low cost, low power request, simple apparatus, and safety for environment with high quality products. The hydrothermal system consist of two mainly parts electrical controller and reaction chamber, all parts are maddened home with global specifications.

ZnO(1g) nanoparticles (particle size about 20-30 nanometer) and Sodium Hydroxide (NaOH) with concentrations 3M, 6M were the starting materials for the chemical reaction under stirring. The suspension was transferred into a Teflon lined sealed stainless steel autoclave and kept at 70 ^{o}C and 90 ^{o}C separately for reaction time 24, 48 and 72hour. ZnO nano structures were successfully synthesized using the concentrations (3M , 6M) of NaOH prepared by hydrothermal method, which provided us with a variety in structure (Nanotubes, nanorods, nanobelts, nanosticks, lettuce leaf, flowers-like, and heterogeneous structures). The experimental pattern of the XRD examinations show that diffraction peaks can be assigned to the Wurtzite hexagonal-shaped ZnO and higher dislocation density for all nanostructures toward the lattice plane (101) excepts the condition 3M NaOH,90 ^{o}C, for all reaction times. The FE-SEM pictures shows the ZnO structures as nanotubes(3M NaOH,70 ^{o}C for 72h, and 6M NaOH,70 ^{0}C,48 h), nanorods(3M NaOH,90 ^{o}C,48h and 6M NaOH,90 ^{0}C, 48h), flowers-like structures(3M NaOH,90 ^{o}C,72 h), lettuce leaf structures(6M NaOH,70 ^{o}C,24h), nanosticks(6M NaOH,70^{o}C, 72h), heterogeneous structures 3M NaOH,70^{o}C,24 h(nanoparticles and multilayers plates), (6M

NaOH,90^{o}C,24h(nanoparticle and nanosheets), while there are no structures recognize for the condition 6M NaOH,90 ^{o}C,72h. The

atomic force microscope (AFM) are showed high roughness reported for the reaction time 72h for 6M NaOH at 70 Ċ,48h for(3M NaOH at 90 ^{o}C, 6M NaOH at 70 ^{o}C, and 3M NaOH at 90 ^{o}C) . The photo luminescence (PL) measurements for ZnO nanotubes and nanorods synthesis show a blue shift indicated an increasing in energy gap and the nano obtained structure.

Table Of Contents

List of Symbols

Symbol	*Meaning*	*Unit*
D,(G.S)	*Crystallite Size*	*Nm*
E_c	*Bottom Of Conduction Band*	*eV*
E_v	*Top of Valence Band*	*eV*
Δ	*Dislocation Density*	$Line^2/m^2$
T_s	*Substrate Temperature*	*K*
T_r	*Transmission*	*%*
T	*Time*	*S*
Θ	*Diffraction Angle*	*Degree*
D	*Thickness*	*Nm*
Λ	*Wavelength*	*Å*
A	*Absorption Coefficient*	cm^{-1}
B	*FWHM*	*Radian*
Y	*Frequency*	*Hz*
E_g	*Energy gap*	*eV*
H	*Plank constant*	*J.s*
C	*Speed of light*	*m/s*
E_p	*the energy of an absorbed*	*eV*
Vs	*volume of the solid particle*	cm^3
∇G_r	*energy gain*	-
A_{SL}	*area of the interface*	cm^2
γ	*interfacial energy*	*eV*
$\in_o$	*dielectric constants*	*F/M*
K_o	*equilibrium constant*	$L^2\ mol^{-2}$

List of Abbreviations

Abbreviation	Meaning
UV	Ultraviolet
TSO	Transparent Semiconductors
CNTs	Carbon Nano Tubes
AFM	Atomic Force Microscopy
FE-SEM	Field Emission Scanning Electron Microscope
QDs	Quantum Dots
VB	Valence Band
CB	Conduction Band
PL	Photoluminescence
NBE	Near Band Energy
GL	Green Luminescence
HCP	Hexagonal
XRD	X-Ray Diffraction
SEM	Scanning Electron Microscopy
EDAX	Energy Dispersive X-Ray Spectroscopy
CRT	Cathode Ray Tube
e-beam	Electron beam
LSW	Shift- Slyszov-Wagnor
FWHM	Full Width Have Maximum

CHAPTER ONE

SCIENTFIC REVIEW

Chapter one

Introduction

In this chapter, was addressed to the characteristics of zinc oxide and methods of preparation, it was also mentioned the importance and benefits of nanoscience and nano-technology. And there is also the historical overview of this chapter, and the theoretical side of the subject.

1.1 Background of ZnO

Nanotechnology has become one of the most important and exciting advance fields in Physics, Chemistry, Engineering and Biology. It shows great promise for providing us in the near future with many fast jumps that will change the direction of technological advances in a wide range of applications [1,2]. The field of nano materials engineering represents an exciting and rapidly expanding research area that crosses the borders among the physical, life, and engineering sciences [3].

Most of the excitement in this domain of research has arisen from the realization that fundamentally new material properties and synthesis of multifunctional materials are possible with structures designed at the nanometer-scale. The research activities represented in these domains are varied, extend from extensions of traditional device physics to completely new approaches based upon molecular self-assembly, from developing new materials with dimensions on the nanoscale to investigating whether we can directly control matter on the atomic scale [4-6]. The interest in nanotechnology is also driven by the fact that the physical and chemical properties of synthetic materials

can significantly improve or largely change as their size is reduced to the nanometer scale. More important, it is now becoming increasingly well realized that the new concepts and applications of nanotechnology are not only limited to the physical science and, indeed, can be applied to the field of life science, medicine, Nano devices and energy production [7].

Several deposition methods have been used to grow undoped and doped ZnO films such as spray pyrolysis, vacuum evaporation, chemical vapor deposition, magnetron sputtering, pulsed laser deposition, sol-gel technique and screen printing technique [8-14]. More recently, there has been significant effort in progress for design and development of ZnO nanostructures such as ZnO nanowires for a variety of applications bulk and thin films of ZnO have demonstrated high sensitivity for toxic gases. The ZnO nanostructures can be implemented in optoelectronic, Sensors, Transducers and Biomedical applications. Use of these nanostructures, will allow building of Nanoscale nanosensors, nanocantilevers, field-effect transistors and nan resonators for a variety of military, Homeland Security and commercial applications. Due to the advancement of materials technology over the past decade, wide-band gap semiconductors such as ZnO have emerged as UV sensitive materials that have applications for UV lasers, UV Photo detector, switches, Bio-Sensors and solar cells. ZnO wide-band gap semiconductor is promising for sensor applications in the UV range .The band-gap is 3.37 eV for ZnO. Therefore, ZnO, is potentially good material to cover the UV spectral band (240-280 nm), when solar radiation is completely absorbed by the ozone layer of the earth atmosphere, so the background of solar radiation at the earth surface is essentially zero. ZnO is transparent to visible light and can be made highly conductive by doping. ZnO is a

multiple functional material that has a multiple group of growth morphologies[15].

These growths morphologies have been demonstrated for nanowires, nanobelts, nanocages, nanocombs, nanosprings, nanorings and nanohelixes. (see figure 1.1)Based on these remarkable physical properties and the prompting of device miniaturization, large effort has been focused on the synthesis, characterization and device applications of ZnO nano materials. An assortment of ZnO nanostructures, such as nanowire, nanotubes, nano rings, and nano-tetrapods have been successfully grown via a variety of methods including chemical vapor deposition, thermal evaporation, and electro deposition, etc.

These nanostructures have been subjected to electrical transport, UV emission, gas sensing, and ferromagnetic doping studies, and considerable progresses have been achieved [16, 17].

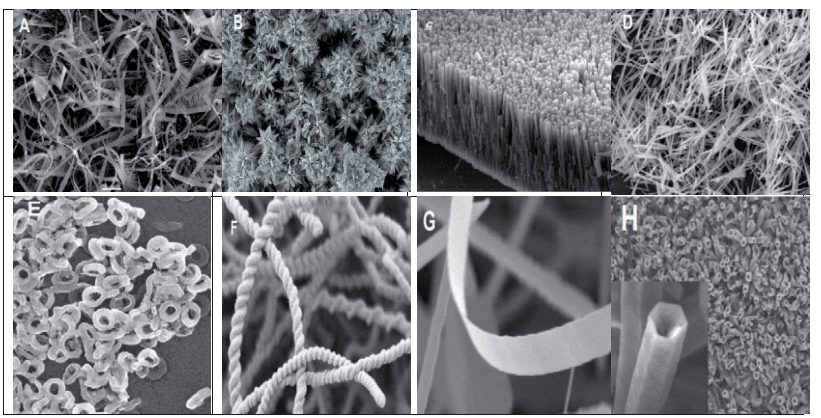

Figure (1.1): ZnO (A) nanocombs, (B)nano flower, (C)nano rod, (D)nanowires, (E)nano rings, (F) nanospring, (G) nanobelts, (H)nanotube [16].

1.3 Nano science concepts

One of the most important thinks is to determine accurate definition and concept: a nanostructure is any structure with one or more dimensions measuring in the nanometer (10^{-9} m) range. Various definitions modify this further, stating that a nanostructure should have a characteristic dimension vary between 1nm and 100nm, putting nanostructures as inter mediate in size between a molecule and a bacterium [18, 19]. In general, we will take a slightly more flexible definition and allow "nanostructure" to include larger structures providing that the object's size of the plays an essential role in determining its physical properties Experimentalists now have access to A large variety of nanostructures, both self-assembled (e.g. fullerenes, nanotubes, and directly fabricated (e.g. quantum wires, lateral quantum dots, etc.). should give an idea of the difference of such structures, as appeared through the techniques of electron and atomic-force microscopy. Thought of as one being big enough to be successfully influence in experiment, and yet small enough to be interesting [20, 21].

1.4 Definition of nanoparticles

The nanoparticles are ultrafine particles in the dimension of nanometer order. "Nano" is a prefix denoting the definition of nano-particles differs depending upon the materials, fields and applications concerned [22]. In the narrower concept, they are considering as the particles smaller than 10-20nm, where the physical properties of solid materials themselves would drastically change. On the other hand, the particles in the three digit range of nanometer from 1 nm to 1m could be called as nanoparticles. In many cases, the particles from 1 to 100 nm are generally called as nanoparticles, but here they will be regarded as the

particles smaller than those called classically “submicron particles”, and specified less than the wavelength of visible light (its lower limit is about 400nm) as a measure, which need to be treated differently from the submicron particles [23, 24].

1.5 Definition of particle size

Practical applications of powder-particles, usually powder is constituted by particles of various sizes and therefore, particle size is the most important information in necessary to obtain not only the mean particle size but also the size distribution for the characterization. Recently the methods for particle size analysis have been greatly developed. Especially, the analyzers with prominent characteristics such as rapid response, high repeatability and covering wide range of particle size are developed as in the case of laser scattering and diffraction method [25].

A particle is usually three-dimensional and it may take various shapes. “Particle size” can be defined as the three-dimensional particle in one-dimensional scalar value. The size of any spherical particle cans be represented by its diameter clearly. For a particle with unequal shape, the size is represented by a geometrically obtained one-dimensional scalar value, geometric size, or an equivalent size in relation to practical methods of particle size measurements [26, 27].

1.6 Attribute of nanoparticles:

1.6.1 Activation of particle surface

All the solid particles made by the atoms or the molecules. As they are micronized, they tend to be affected by the behavior of atoms or the molecules themselves and to show different properties from those of the bulk solid of the same material. It is attributable to the change of the

bonding state of the atoms or the molecules building the particles. The diameter of the smallest hydrogen atom is 0.074 nm, and that of the relatively large lead atom (atomic number is 82) is 0.35 nm. From these sizes, it is estimated that the particle with a size of 2 nm consists of only several tens to thousands atoms. When the particle is constructed by larger molecules, the number decreases furthermore, it is indicated that the fraction of surface atoms of a 20 μm cubic particle is only 0.006% but it increases to 0.6% for a 200 nm particle and then it is estimated almost half of the atoms are situated at the surface of a 2 nm particle [28].For example, as shown in figure (1.2), if a cube with a side length of 1 cm is divided into a cube of 1 μm, the particle number increases to 10^{12} and being divided into the one of 10 nm, then it amounts to 10^{18} where the fraction of the atoms or the molecules located at the surface on the particles plays a great role, since they are more active than those inside the solid particles because of the free hand, which leads to easy bonding with the contacting materials and causes various changes in particle properties .

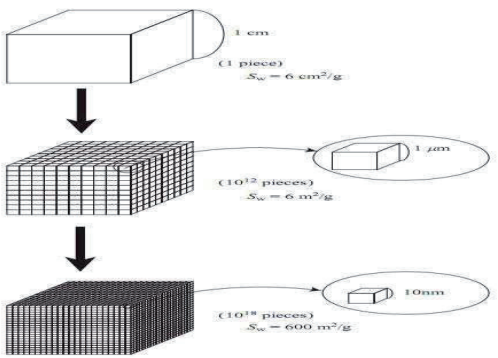

Figure (1.2) Activation of surface area [23]

1.6.2 Increase of surface area

The specific surface area increases generally in reversal proportion to the particle size. In the above-mentioned case, when the particle of 1cm is micronized to 1μm and 10nm, the specific surface area becomes ten thousand times and million times, respectively. As the increase in the specific surface area directly influences such properties like the solution and reaction rates of the particles, it is one of major reasons for the unique properties of the nanoparticles different from the bulk material together with the change in the surface properties of the particles itself.

1.7 Zinc oxide properties

Zinc oxide (ZnO) is a well-known wide band gap semiconductor 3.37 eV with excitation energy 60meV at room temperature. Also ZnO is one of the transparent semiconductors(TSO) with high melting point(1970˚C) Which has a wurtzite structure with a lattice parameter a = 0.325 nm and c=0.512 nm. The distance between Zn ion and O_2 ion along the c-axis is 0.1992 nm, and the distance between these two ions along other three axes is 0.1973 nm (as show in table 1.1)[29]. The two major characteristics of the ZnO structure are the non-central symmetry and polar surfaces. The structure of ZnO can be described as a number of alternating planes composed of tetrahedral coordinated O^{-2} and Zn^{+2} ions which are stacked alternately along the c-axis as shown in figure (1.3) [30].

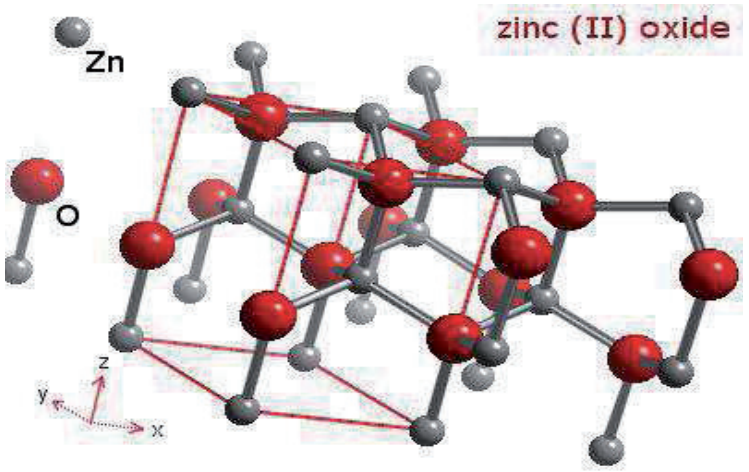

Figure (1.3): The hexagonal structure of ZnO showing the arrangement of Zn^{+2} and O^{-2} atoms [30]

The oppositely charged ions produce positively charged-$Zn^{+2}$and negatively charged O^{-2} Polar planes, which result in a normal dipole moment and spontaneous polarization along the c-axis and different surface energy with the different crystallographic orientations as in Figure (1.4).

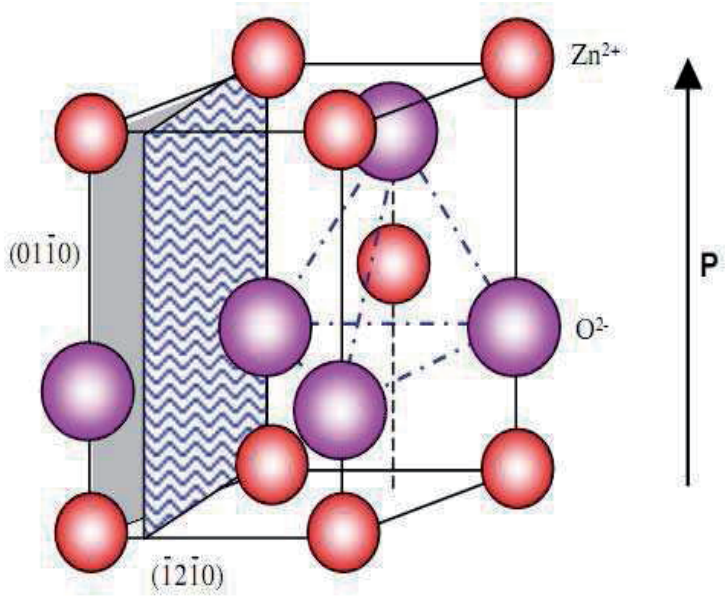

Figure (1.4): The tetrahedral coordination of ZnO [31].

ZnO thin films generally exhibit a good optical transmission (over 80%) in the visible and near infrared wavelength range due to its wide band gap energy [31-33].

This transmission value of ZnO thin films depends on its microstructure and roughness[34].

Table(1.1) physical properties of ZnO[29]

Properties	ZnO
Lattice parameters at 300 K —a_0 (nm) —C_0 (nm) —C_0/a_0	 0.32495 0.52069 0.65032
Density (g/cm^3)	5.606
Stable phase at 300 K	Wurtzite
Melting point (C)	1975
Thermal conductivity ($Wcm^{-1} c^{-1}$)	0.6, 1-1.2
Linear expansion coef? cient (C)	$a0$: 6.5×10^{-6} $c0$: 3.0×10^{-6}
Static dielectric constant	8.656
Refractive index	2.008
Band gap (RT)(eV)	3.370
Band gap (4 K) (eV)	3.437
Exaction binding energy (MeV)	60
Electron effective mass	0.24
Electron Hall mobility at 300 K (cm^2/Vs)	200
Hole effective mass	0.59

1.8 Estimation of nanoparticles size

In order to explain the change in properties and characteristics of nanoparticles with the particle size it is essential first of all to measure the size of the nanoparticles accurately. The fundamental method to measure the size of nanoparticles is the size analysis from the picture image using the transmission electron microscope, which could also give the particle size distribution. For this analysis, preparation of the well-dispersed particles on the sample mount is the key issue. The grain size of the particles can be obtained from peak width at half height in the X-ray diffraction analysis and it is regarded as an average primary particle size of particles [35].

1.9 Advantages of Nanostructured Morphology

Nano crystals can be loosely defined as crystals with dimensions up to 100 nm; above this size, they are more commonly termed microcrystals. QDs are nanocrystals that display quantum size effects. While there are different quantum size effects with different size scales, the term is commonly understood to refer to nanocrystals whose dimensions are smaller than the bulk Bohr diameter of the semiconductor - typically several nm up to several tens of nm. In this size system, as the crystal size becomes smaller the semiconductor energy levels become more separated from each other and the effective band gap increases, This means that a material with a fixed chemical composition and crystal structure can be made to have very different optoelectronic properties solely by virtue of its physical dimensions. It is largely this property that has generated the high level of interest in the field [36- 39].

1.10 Synthesis techniques

The common materials synthesis procedures can generally be grouped in two different categories, the top-down' 'approaches and the bottom-up approaches. In this section, these two approaches are briefly discussed with respect to the synthesis of 1D nanostructure.

1.10.1 Top-Down Synthesis

The top-down approaches usually utilize planar, lithographic, etching, and deposition techniques to transfer a pre-designed pattern to a substrate which can form complex high density structures in well-defined positions on substrates and their integrated systems. The top-down approach has been exceedingly successful in extensive applications, with microelectronics being perhaps the best example today [40].

They can produce 1D nanostructure with very uniform shapes and electronic properties. While developments continue to push the resolution limits of the top-down approach, these improvements in resolution are associated with a near-exponential increase in cost associated with each new level of manufacturing facility [41, 42].

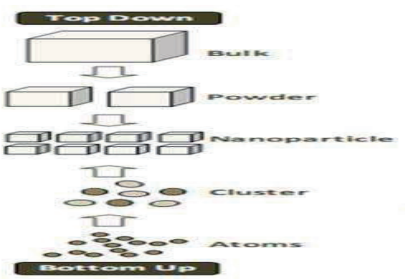

Figure (1.5): Schematic explains the formation of nanostructures via top-down and bottom-up approaches [41].

1.10.2 Bottom-Up Synthesis

The bottom-up approach, in which functional structures are assembled from well-defined chemically and/or physically synthesized nanoscale building blocks, much like the way nature uses proteins and other macromolecules to construct complex biological systems, represents a powerful alternative approach to conventional top-down methods. [43].

To enable this bottom-up approach for nanotechnology requires a focus on three key areas that are at the heart of devices and integration. First, the bottom-up approach necessitates nanostructured building blocks with precisely controlled and tunable chemical composition, structure, size, and morphology, since these characteristics determine their corresponding physical properties. Meeting this goal demands methods that enable rational design and predictable synthesis of building blocks. Secondly, it is critical to develop and explore the limits of functional devices based on these building blocks. 1D nanostructures may behave in ways similar to current electronic and optoelectronic devices, although it is also expected that new and potentially revolutionary concepts will emerge from these building blocks, for example, due to quantum properties, third and central to the bottom-up concept will be the development of architectures that enable high-density integration with predictable function, and the development of hierarchical assembly methods that can organize building blocks into these architectures [44-46].

1.11 Simple Evaporation Techniques

In principle, the thermal evaporation technique is a simple process in which condensed or powder source material is vaporized at elevating temperature and then the resultant vapor phase condense under certain conditions such as (temperature, atmosphere, substrate etc.) to form the desired product. The processes are usually carried out in a horizontal tube furnace, as shown in figure (1.6), which is composed of a horizontal tube furnace an quartz tube, a gas supply and control system. The right-hand end of the quartz tube is connected to Argon and oxygen container. The flow rate was controlled by two flow meters. The left end of the tube is lefted free. The row material (metal) is putted in an alumina boat and positioned at the center of the quartz tube, where the temperature is the highest. Substrates were placed downstream for collecting growth products. This simple set-up can achieve high control of the final product[47,48].

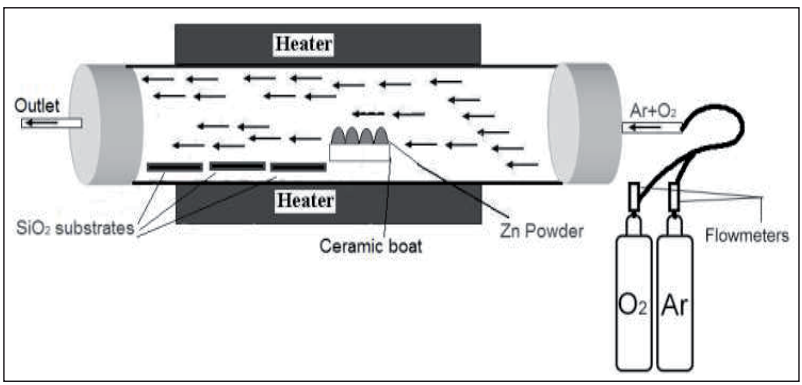

Figure (1.6): Schematic of simple evaporation system [47].

1.12 Aqueous Chemical Growth

Solution chemistry based and wet chemical techniques represent the most low coast and simplest technique to produce 3-D arrays on a large domain. They will participate and give enhancement to the manufacturing of raw nanostructures and play a major line in the fabrication of practical nano devices. Such methods are template based synthesis, electro deposition techniques, and aqueous chemical growth [49].

This novel technique has emerged recently as a simple and powerful tool to fabricate, at low cost and low temperatures, large areas of metal oxide nano to micro particulate thin films. 3D arrays consisting of orientated with different properties nanoparticles are easily synthesis with enhanced control over the orientation and the dimensions. The synthesis involves the controlled hetero nucleation of metal oxides in aqueous solutions [50-52].

1.13 Hydrothermal synthesis

Hydrothermal synthesis includes various techniques of crystallizing substances from high temperature aqueous solutions at high vapor pressures; also termed "hydrothermal method". The term "hydrothermal" is of geologic origin. Geochemists and mineralogists have studied hydrothermal phase equilibrium since the turn of the century. George W. Morey at the Carnegie Institution and later, Percy W. Bridgman at Harvard University did much of the work to lay the foundations necessary to containment of reactive media in the temperature and pressure range where most of the hydrothermal work is conducted for the process occur at an optimal rate Hydrothermal synthesis can be defined as a method of synthesis of single crystals which

depends on the solubility of minerals in hot water under high-pressure see figure (1.7) The crystal grow this performed in an apparatus consisting of a steel pressure vessel called autoclave, in which a nutrient is supplied along with water. A gradient of temperature is maintained at the opposite ends of the growth chamber so that the hotter end dissolves the nutrient and the cooler end causes seeds to take additional growth [53].

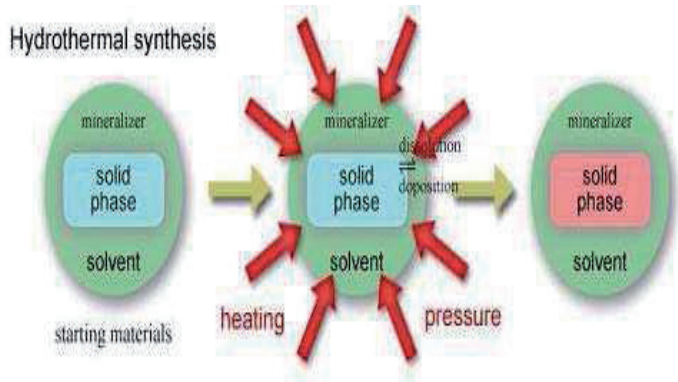

Figure (1.7): The process of hydrothermal synthesis, reviling the importance of pressure and heat [53].

The super saturation is the most widely used method in hydrothermal synthesis and crystal growing. The super-saturation is obtained by lowering the temperature in the crystal growth zone [54].

A hydrothermal synthesis is a special case of a solvothermal process, which is generally defined as a chemical reaction taking place in a solvent at temperatures above the solvent boiling point and at pressures above 1 bar [55].

The hydrothermal method exploits that by increasing temperature and pressure, the fundamental properties of water and thus its abilities as a solvent changes

The precursor used in the synthesis of inorganic compounds is often aqueous solutions of simple salts such as metal chlorides, nitrates or

acetates. Depending on the specific synthesis, these can be precipitated to the corresponding metal hydroxides prior to the synthesis using a base (often NaOH, KOH or NH_4OH), and other additives for e.g. pH control, reduction or oxidation, coating etc. can equally be added prior to the hydrothermal treatment. The reaction mechanisms are naturally highly system dependent, but when considering a simple and classic example, namely the synthesis of metal oxide particles, adschiri et al have in 1992 suggested the following 2-step formation mechanism for particles from a simple metal salt [56]:

Step 1: Hydrolysis $MXx\ (aq) + xH_2O\ (l) \longrightarrow M\ (OH)x(s) + xHX$

Step 2: Dehydration $M\ (OH)\ x(s) \longrightarrow MO_x/_2(s) + x/2\ H_2O$

Here, M denotes the metal and X the anion. As the temperature is increased, the equilibria shift to the right, leading to the formation of metal oxide particles. However, even in this simple example, several aspects of the reactions are not known. The intermediate phase $M\ (OH)_x$ is hard to characterize as the second reaction often happens quickly after the formation

of the hydrated phase. Furthermore, as the intermediate phase is often amorphous and nano-sized, it is difficult to obtain structural information from traditional characterization methods. The mechanisms controlling the reactions are thus not well understood[57]

1.14Optical Absorption and Absorption Edge

The absorption process is fundamental property of semiconductors which involves the transition of electrons from the valence to the conduction band, which apparent itself by a rapid rise in absorption and this can be used to determine the energy gap of the semiconductor [58].

The semiconductor absorbs photon from the incident beam, the absorption depends on the photon energy ($h\nu$); where h is Plank′s constant, ν is the frequency of incident photon, the absorption is related with the electronic transition between the V.B. and the C.B. in the material starting at the absorption edge which corresponds to minimum energy difference (E_g) between the lowest minimum of the C.B. and the highest maximum of the V.B. If the photon energy ($h\nu$) is equal or more than energy gap (E_g) then, the photon can interact with a valence electron, elevates the electron into the C.B. and creates an electron–hole pair [59]. The maximum wavelength (λ_c) of the incident photon which creates the electron–hole pair is defined as [59]:

$$\lambda\ (\text{nm}) = \frac{hc}{E_g} = \frac{1240}{E_g(\text{eV})} \quad (1.1)$$

1.15 Photoluminescence Spectroscopy

The word band is used because the electrons have a multiplicity of energies in either band Furthermore, there is an energy gap between the conduction and valence electron states Under normal conditions electrons are forbidden to have energies between the valence and conduction bands If a light particle (photon) has an energy greater than the band gap energy, then it can be absorbed and thereby raise an electron from the valence band up to the conduction band across the forbidden energy gap as shown in figure (1.8) In this process of photo excitation, the electron generally has excess energy which it loses before coming to rest at the lowest energy in the conduction band. At this point the electron eventually falls back down to the valence band [60-61]. As it falls down, the energy it loses is converted back into a luminescent photon which is emitted from the material. Thus the energy of the emitted photon is a

direct measure of the band gap energy, Eg. the process of photon excitation followed by photon emission is called photoluminescence.

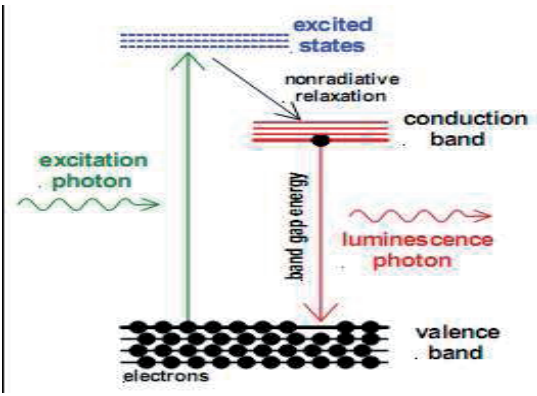

Figure (1.8): Photoluminescence phenomena [61]

ZnO is well known to possess remarkable optoelectronic properties. From room temperature PL investigations this material shows a sharp Near band Energy (NBE) emission peak in the UV region and a broad green luminescence (GL) emission peak in the visible range which is related to the defects Consequently, the electrical photo conduction should be modulated according to the photo excitation with wavelengths in the UV and the visible range, The finger grid structure with multiple ZnO nanowires is investigated to detect the photo response of ZnO nanowires for different wavelengths.

To get information about the optical properties of this ZnO nanowire device the PL spectrum was taken for the wavelength range between 350 nm and 700 nm figure (1.9). For photo excitation a Xe-lamp possessing a wavelength of 325 nm and power of 30 mW was used [62].

From these PL data (normalized to the NBE peak intensity) the nanowires exhibit a rather weak green luminescence compared to the NBE peak. This suggests that the nanowires are of relatively high quality due to the strong NBE.

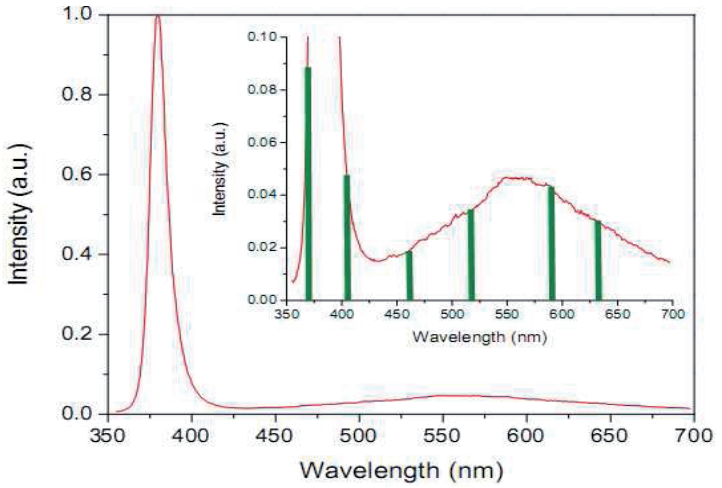

Figure (1.9): PL for ZnO [62].

In the inset of figure (1.9) the NBE and GL peaks are magnified and wavelengths of interest for the electrical photo response investigations are marked with the green bars. The values are chosen to cover the visible range below the band-gap of ZnO and a wavelength with an energy (>400nm) above the band-gap. Therefore, the device is excited with 465 nm (blue), (590 nm) yellow, and 630 nm (red) wavelengths in the visible range and with 370 nm whose energy is slightly higher than the band gap energy. In case the device is illuminated, the density of photo generated carriers (Δn) result into an increase in photo conductance (G) [63,64].

1.16 Dislocations Density

The number of dislocations in a material is defined as the dislocation density - the total dislocation length per unit volume or the number of dislocations intersecting a unit area. Dislocations exists in Most crystalline materials, especially metals, have dislocations in their as-formed state, mainly as a result of stresses (mechanical, thermal...) associated with the formation process The number of dislocations increases dramatically during plastic deformation Dislocations seed from existing dislocations, grain boundaries and surfaces [65,66].

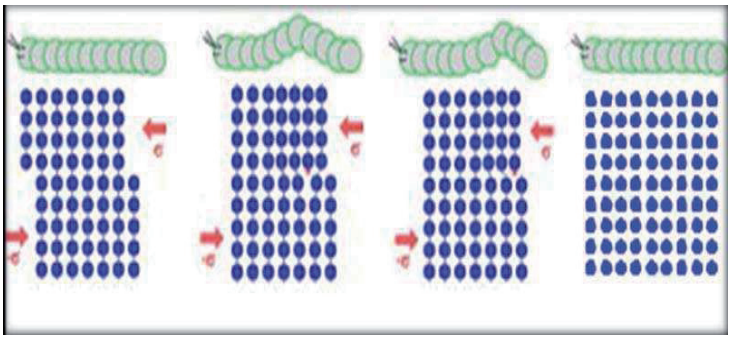

Figure (1.10): dislocation motion [65].

If the top half of the crystal is slipping one plane at a time then only a small fraction of the bonds are broken at any given time and this would require a much smaller force [67]. The propagation of one dislocation across the plane causes the top half of the crystal to move (to slip) with respect to the bottom half but we do not have to break all the bonds across the middle plane simultaneously (which would require a very large force The slip plane- the crystallographic plane of dislocation motion Dislocations allow deformation at much lower stress than in a perfect crystal.

1.17 Particle Nucleation and Growth Theory

1.17.1 Nucleation of Particles in a Liquid

Classic, nucleation theory builds on theoretical considerations for solid particles in melts, but these are often extended to other solid/liquid systems e.g. hydrothermal synthesis. Although many approximations are done when considering a hydrothermal synthesis in this context, the approach is useful when trying to understand the basic processes. The theory uses simple thermodynamic functions to describe the formation of the nuclei that lead to particles. Two different mechanisms are often considered, namely homogenous or heterogeneous nucleation, and here, homogenous nucleation is introduced [68].

Generally, atoms in a melt (or another liquid phase) will fluctuate in the liquid phase due to thermal motion. Sometimes, these fluctuations will lead to formation of atomic assemblies with local structures resembling that of a solid phase. If there is a thermodynamic gain related to this cluster formation, the assembly might stay stable, and act as nuclei for particle formation. However, when forming a new particle, an interface between the liquid and solid phase is created. This costs energy, and the total expression for the change in Gibbs free energy can be written as:

$$\Delta G_r = -V_s \Delta G_v + A_{sl}\,\gamma_{sl} \qquad (1.7)$$

Here, Vs is the volume of the solid particle, ∇G_r the energy gain by forming the solid, A_{SL} the area of the interface and γ the interfacial energy. Assuming that this energy is isotropic and that the particles are spherical with radii r, the following expression is obtained:

$$\Delta G_r = -\frac{4}{3} r^3 \Delta G_v + 4\pi r^2 \gamma_{SL} \qquad (1.2)$$

This function is plotted in figure (1.11), where a maximum is seen at

$r = \frac{2\gamma SL}{\Delta Gv}$ (1.3).

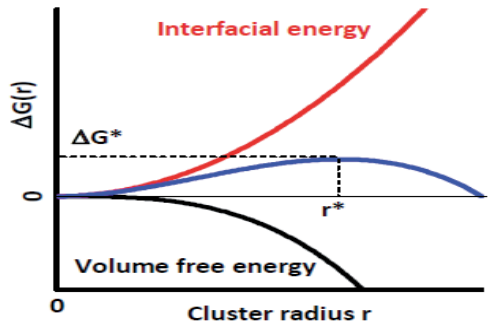

Figure (1.11): The size dependent change in Gibbs free energy for nucleation as function of the radius of the formed of solid cluster [68].

Thus, only above this limit, it is thermodynamically favorable to form particle nuclei. Below it, the clusters are unstable in equilibrium with the species still in solution. The local fluctuations and the amount of species in the liquid phase therefore have to be large enough for clusters above the critical size to form [69].

1.17.2 Growth of Particles in Solution

When stable nuclei have formed in the liquid, the particles will start growing to minimize the energy loss related to the newly formed high surface area. This can happen through several different growth mechanisms, again depending on the chemistry and local environment. Classically, particle growth is described based on differences in surface energy of small and large particles.

For solid species present at a solid/liquid interface, the chemical potential increases with decreasing particle size, following the thermodynamic theory presented above. This leads to re-dissolution of

the smallest, newly formed particles, creating a concentration gradient in the solution. Uniformity of the concentration is reestablished by material diffusion towards the larger particles, thus leading to particle growth. The process, illustrated in a simple diagram in figure (1.12), was first described by ostwald in 1897 and the mechanism is therefore known as 'ostwald ripening'. Since the growth rate is dictated by material diffusion between particles, the process is often termed 'diffusion limited growth [70-80].

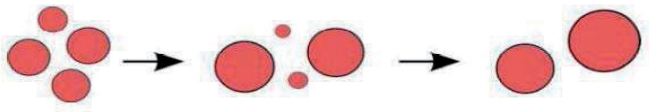

Figure (1.12): Particle growth by ostwald ripening [72].

1.18 Literature Review

Yongnan and Young, (2004), prepared ZnO nanorods using hydrothermal method by using metallic zinc powder (100 mesh, Aldrich) as the raw material. Typically, 0.4 g of Zn powder and 14mL of H_2O were mixed in a Teflon vessel without stirring. Then 1mL of H_2O_2 (35%) was injected. The mixture was sealed and hydrothermally reacted at 220^oC for two days. The structural properties of the powder. The nanorods are single crystalline that have pencil-like morphology with sharp ends. The formation of zinc oxide nanorod arrays is influenced by the reaction temperature and the form of zinc metal[81].

Yong, et al. (2005), synthesized ZnO nanorods with the mean size of 50 nm×250 nm were successfully via a hydrothermal synthesis route in the presence of cetyltrimethylammonium bromide (CTAB). $ZnCl_2$ and

KOH were used as the starting materials**,** with simple system at 120 ◦C for 5 h.$ZnCl_2$ and KOH were used as the reactants and CTAB as the directed reagent for growth of ZnO. The absorption peak of the as-obtained ZnO nanorods has a slight blue-shift compared with that of the bulk. Experiments showed that the different zinc source and reaction temperature would influence morphologies and absorption properties of the final products but the PL spectra not change generally [82].

Liu, et al. (2006), various undoped/Cd-doped ZnO nanostructures have been synthesized through a simple evaporating method, undoped/Cd-doped ZnO nanostructures were synthesized on gold particles-filled AAO templates via a simple controllable thermal evaporation process. Under different growth conditions, the undoped ZnO products could be pure nanowires, pure nanobelts, or a farrago of microcombs nanobelts and nanowires. Using catalyst-free graphite sheet as substrate, ZnO nanowires together with comb-like structures were obtained. The Cd-doped ZnO nanostructures grown on the AAO substrates covered with gold catalysts could be nanowires. The structural properties studied with x-ray and (SEM) and the optical properties with (PL) [83].

Oleg, et al, (2008) prepare ZnO nanorod using hydrothermal method. Starting materials are analytical grade zinc sulfate ($Zn(SO_4).7H_2O$) and ammonia solution (NH_4OH) from Fisher Scientific. Rapid thermal processing of grown ZnO nano architectures at 600^oC for duration of 60 s was realized. Rapid thermal annealing in 30–60 s after synthesis of ZnO nanorods determine desorption of the large number of chemisorbed oxygen species at the surface of freshly prepared zinc oxide samples. The loss of adsorbed oxygen increases the electron concentration of the surface and improves the conductance. The major advantages of this method are its simplicity and fast growth rates (10 min versus several hours). They also showed that the morphology and distribution of

nanorods can be effectively controlled by using suitable preparing conditions. In addition, an in-situ lift-out technique has been presented to fabricate single ZnO nanorod H_2 sensor. [84].

Yousefi, et. al., (2009), studied the electrical and structural properties of different ZnO structure prepared by hydrothermal method FESEM images and XRD patterns of the ZnO nanostructures, which were grown on various substrates that were placed at different positions in the furnace: thin nanowires (d ≈ 90 nm) at 650 °C (a), thick nanowires (d ≈ 300 nm) at ~ 600 °C (b), and a mixture of nanodiscs with a wide distribution of diameters (800 nm ≤ d ≤ 4 μm) at ~ 550 °C (c). It can be seen that, the formation of various ZnO nanostructures is only mixed for the sample that was placed at the furthest distance from the source material. Nanostructures with different sizes were obtained in the different regions of the tube [85].

Ahn,et. al. (2009), prepared ZnO nanowire by used graphite as catalyst with ZnO powder, the mixture thermally evaporated and the ZnO nanowires screen printed for gas sensing. ZnO-nanowire gas sensors, in which nanowire bridges were, self-assembled between two electrodes by a selective growth of ZnO nanowires on patterned Au catalyst layers. The sensors demonstrated high gas response to NO_2 down to sub-ppm level and fast response/recovery behaviors. The gas response showed a maximum value at 225◦C and linearly increased with the concentration of NO_2 in the range of 0.5–3 ppm and then saturated afterward. The sensor has similar or even higher response compared with different types of sensors: ZnO nanocrystals, Sn- and In-doped ZnO thin film, or ZnO nanowires. Also, the shorter recovery time than those of previously reported nanobelt based gas sensors was explained by the fact that ZnO nanowires are floated above the substrate and thus the adsorbed

molecules can be easily desorbed from the surface of ZnO and swept away from the gas sensor [86].

Lv, et. al. (2010),prepare ZnO nano/microstructures which formed by using ZnO powders mixed with carbon group elements (C, Si, Ge, Sn, or Pb) as the reducing agent. For cases of mixed precursors of ZnO/C, ZnO/Si, and ZnO/Ge, the pure ZnO nano/microstructures are realized, while for ZnO/Sn (ZnO/Pb) systems, the phase of $Pb_2O_3(Zn_2SnO_4)$ generally are represented in the ZnO products. The appearance of $Pb_2O_3(Zn_2SnO_4)$ is attributed to the lower melting point and higher vapor pressure of Sn (Pb) in the heating and evaporation processes. The morphologies and sizes of the products are controlled by adjusting the growth regions and/or introducing gaseous argon. Room temperature (RT) photoluminescence spectra indicate that the intensity (peak position) of the ultraviolet emission is increased (redshift) due to the existence of Zn_2SnO_4 phase in the ZnO products. The $Pb_2O_3(Zn_2SnO_4)$ phase in ZnO nano/microstructures plays an important role in enhancing the saturation magnetizations of RT ferromagnetism with respect to the case of pure ZnO products fabricated by the precursor of mixed ZnO and graphite [87].

Kang, et. al.,(2011), highly crystalline ZnO hierarchical nanostructures were prepared at room temperature through the alkaline hydrolysis of zinc salt by the forced mixing of two immiscible solutions: Zn-nitrate aqueous solution and oleic-acid-dissolved n-hexane solution. The oleic acid acted as a surfactant in the room-temperature formation of well-defined ZnO hierarchical nanostructures, which subsequently demonstrated a sensitive and selective detection for C_2H_5OH of the screen print films. The responses of these hierarchical nanostructures to 10–100 ppm C_2H_5OH ranged from 15.7 to 177.7, which were 7–9 times higher than those of the agglomerated nanoparticles [88].

Shao and Jeong, (2013),Sheet-like ZnO nanostructure was successfully synthesized through a simple, cost-effective, and low temperature sonochemical process followed by an etching treatment in an alkali environment at room temperature without any catalyst,. The morphology and crystallinity of the products were examined by X-ray diffraction (XRD) analysis, scanning electron microscopy (SEM) and transmission electron microscopy (TEM). The as-prepared nanosheets with high purity were single crystals and well-dispersed. Micro gas sensor fabricated from the as-prepared ZnO nanosheets were tested to different concentration of volatile organic compounds (VOCs) gases. The gas-sensing results revealed that ZnO nanosheets-based micro sensor exhibited high sensitivity to acetaldehyde and formaldehyde with response time within 10 s and the detection limit down to 50 ppb. The excellent sensing property of ZnO nanosheets is mainly attributed to their large specific area, accessible surface, and less agglomerated configuration [89].

Jian-Fu, et. al., (2014), this study developed a hydrothermal method for the growth of three types of zinc oxide (ZnO) nanostructure: nanorods, nanowalls and nanoflowers. The structures are produced at high densities with a high degree of uniformity on Al coated SiO_2 substrates without the need for surfactant. Unlike the random distribution of ZnO nanoflowers reported in previous studies, the proposed method makes it possible to control the distribution of these structures along grooves created by altering the growth rate of ZnO nanorods and nanowalls. The number of ZnO nanoflowers created in this manner depends on the concentration of solution (HMT: hexamethylenetetramine) and reaction time. Measurements of cathodoluminescence (CL), X-ray diffractometry (XRD), and SEM-EDS confirm that the resulting stuctures are pure ZnO with good

crystallinity. We also investigated the optical properties of these ZnO nanostructures and propose a possible growth mechanism [90].

Thamir (2014), study the important application of ZnO nanostructure such as hydrogen gas sensor and getting the high response from the annealed ZnO film interpreted that with oxygen-vacancy model [91]

Huiquan et. al., (2015) synthesized ZnO nanowire array films, composed of well-aligned ZnO nanowires with about 200 nm in diameter and 1 mm in length, were successfully synthesized on Mg-doped gallium nitride by hydrothermal method. The films possess quite flattened surface. In the synthesized process, there was no catalyst used. Growth conditions are comprehensively discussed in the process of aqueous solution method. It was found that the length of ZnO nanowires and the thickness of the film could be tunable by altering solution concentration and growth time. Such ZnO film assembled of vertically aligned nanowire may have potential applications as UV light-emitting diodes [92].

1.19 Aims of the work

The aims of this research are to: 1- prepare of various nanostructures in a manner during hydrothermal method . 2- Study of its properties such as growth ,crystallization, morphology and structure making important class of materials in the development of device that can be used in various application such as : photo-thermal therapy , bio sensors , optoelectronics device , solar cells, cooling system , chemical sensor, nanophotonics device etc.

CHAPTER TWO

PREPARATION AND EXAMINATION SYSTEMS

Chapter two

2.1 Introduction

On viewing the latest international literature researches on the project, an extended background of the experimental research requirements has been acquired. At the beginning of this chapter, a detailed description of the sample preparation technique and the chemicals exploited in samples preparation will be presented. In addition, the experimental set up that has been specially fabricated for the project is outlined. Furthermore, the equipment used are also depicted.

2-2 Outline of the Experimental Project

A block diagram in figure (2.1) shows the practical steps of the present project. It includes the chemical materials whose characteristics are summarized in tables (2.1), (2.2), tables contain various chemicals used in the research and its purity and its industry, as well as materials that have been the industry, including the system in addition to the physical apparatus in which the sample that was prepared in that system were measured and sample preparation by technique chemical reaction. The characterization studies are (X-Ray Diffraction**,** Scanning Electron Microscopes (SEM), FE- Scanning Electron Microscopes ,and Atomic Force Microscope (AFM).

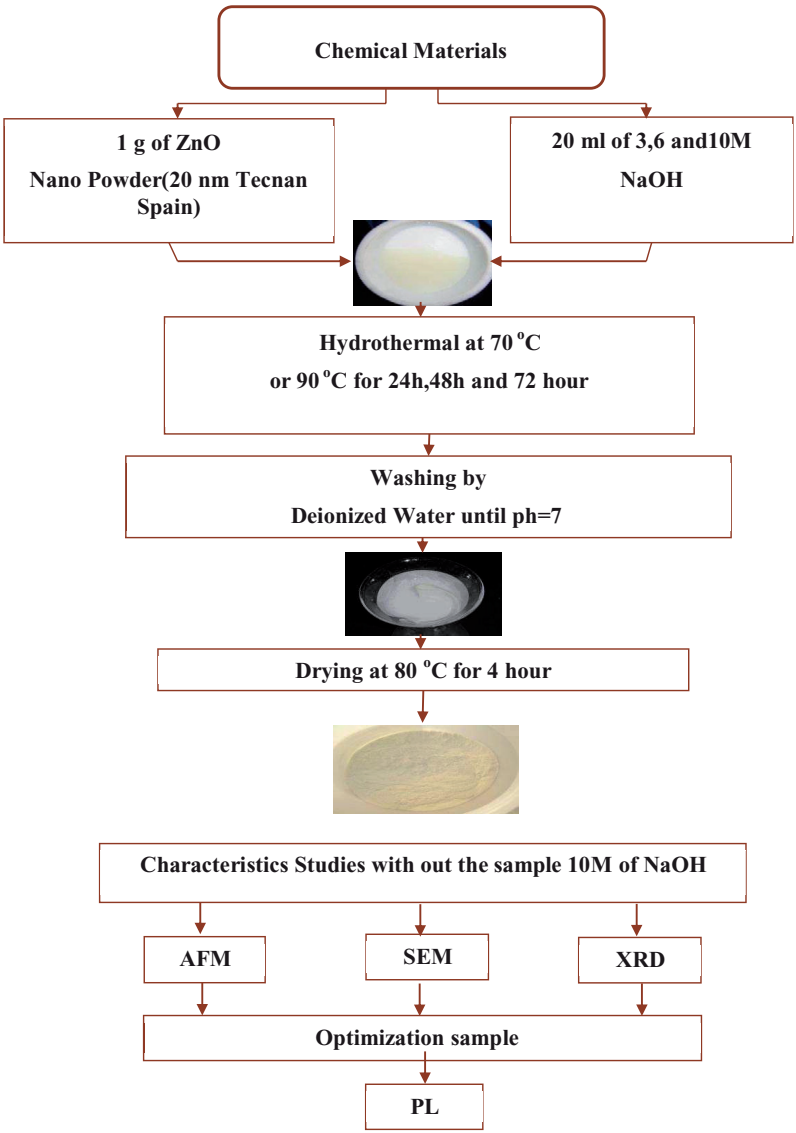

Figure (2-1): A block diagram illustrating the experimental project outline.

Table (2.1): Chemical Materials used in this work.

Item	Material	Origin	Specification
1	ZnO Nano-Powder	Tecnan Spain	99.983 %; particle size 20-30 nm ;specific surface area 35-50 m^2/g ; true density 5.6 g/cc
2	NaOH	Sigma Aldrich Company, Germany	98 % ; Pellets
3	Deionized Distilled Water	Utilities Lap University of Baghdad	Conductivity 10 µm/cm
4	Ethanol	China	99.7% Pure
5	Acetone	BDH	99.7% Pure
6	Hydrochloric Acid (HCI)	Sigma Aldrich	37%
7	Ethylene Glycol	Anhydrous, Sigma Aldrich	99.8%

Table (2.2): Function, origin and specification devices

Item	Device Type	Function	Origin	Specification
1	Ultrasonic Cleaner	Ultrasonic Cleaner	China	Ultrasonic Cleaner With Digital Timer
2	Magnetic Stirrer	Agitation	Germany	220V, 50Hz, 415 Watt Stirrer and Heater Digital Timer/Heater
3	Power Supply	Voltage Source	GW Instek, PSP-603	Voltage Maximum 120 V, 5 Ampere
4	Ovometer	Current Measurement	Taiwan	Measurement of (Voltage, Current, Resistance)
5	Recorder	Voltage Recording	Siemense 8800	-
6	Non-Stirred High Pressure S.Steel Vessel	Hydrothermal Procedure	Homemade	100 ml Teflon Stainless Steel Bomb
7	AFM	Analysis and Characterization	AA3000, Angstrom Advanced Inc. USA	220V, Resolution: 0.26 nm Lateral, 0.1nm Vertical Precision of 50 nm
	SEM		(1)Hitachi FE-SEM Model S-4160, Japan(Tehran university) (2) SEM in ministry of science and technology	(1)0.5 - 20 kV
	XRD		Germany	20 kV, 30 mA
	PL		Germany (Tehran university)	**Perkin Elmer *Spectrophotometer Luminescence LS 55 equipped with FL Win lab software*.**

2.3 Hydrothermal system

The system which is consist of two part they are linked to each other directly, we can of the plate electrical control which is already associated with a fitted 220 (volt) A.C can control at a temperature crucible through heater wraps around it by changing the voltages from 1-220 volt the increase of the temperature of heater (3000W) and thus increase the degree of melting pot heat and also come out of the plate thermal control sensor is placed inside the crucible and this is very important where the sensor turns off when it reaches the desired temperature and cooled crucible while the system is working again.

Now the industry and the parts of the system used to prepare the samples which consist of two parts:

2.3.1 Controller System

they will come to this part of the system and explain it in detail where it was the work of the painting completely homemade, had previously pointed out that this panel that controls the voltage running on heater , the electrical system has a device that measures temperature, this device stores the required degree of the heat on for example 90 °C.

When the temperature of the crucible up to that degree will the device separates through contactor tied with the temperature detected in the thermal sensor, and also it contains a voltmeter voltages appear to be developed and in addition to being overwhelmed at limiter and key works and extinguish the key to control voltages and shows the center of the control panel. As shown in figures 2.2, 2.3:

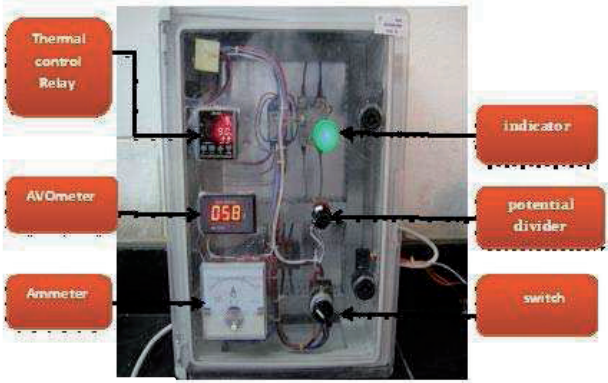

Fig 2.2 : Image of the electronics part device of the system.

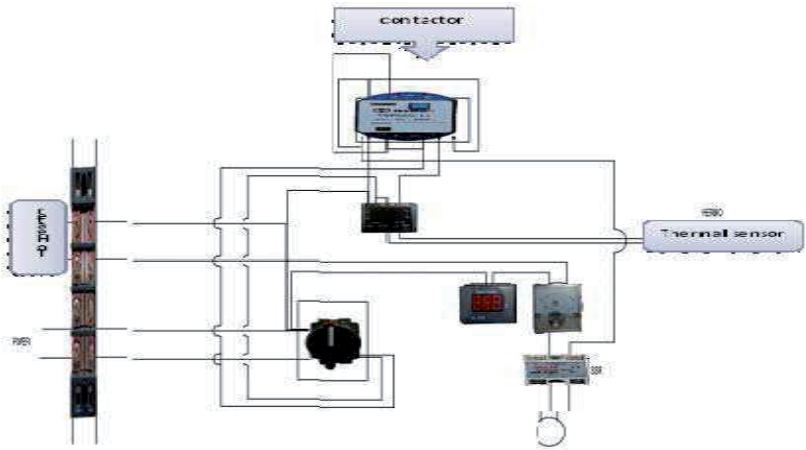

Figure (2.3): Block of the electronics part device of the system.

2.3.2 Stainless Steel Cell

This part contains a device for measuring the pressure extends into the container of Teflon, also has a place dedicated to the development of the thermal sensor and this is a bolt pierced from the center of the place until the introduction of sensor. it reads the temperature inside,(Different with room temperature), when they want to sample preparation we open the bolts the four shown in the figure below and then we derail pot Teflon

and clean it well with chemicals and we are developing material, and then return the pot Teflon inside the stainless steel container and we close the well bolts to prevent the liquid that will become vapor leakage and high pressure up to 11 bar, it should be noted that the pot Teflon expands to 100 ml, heater been wrapped around the crucible in a regular format in order to evenly distribute the heat is on(2.4).

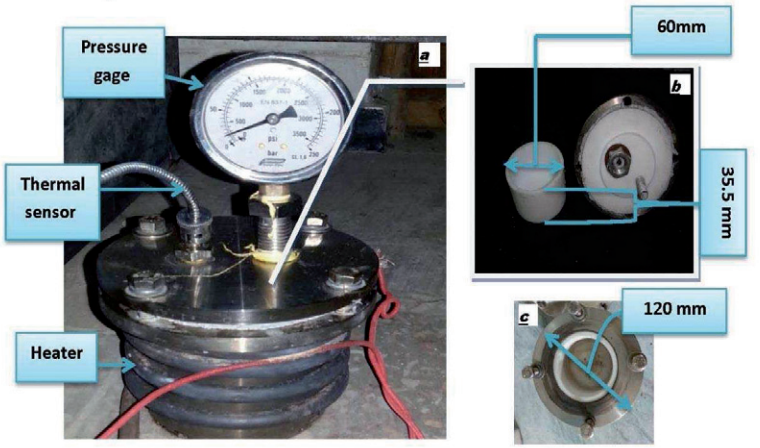

Fig. 2.4 shows the stainless-steel cell a: side view b:inside view

2.4 Hydrothermal Procedure for Synthesis of ZnO nanostructure :

The experiments conducted to convert ZnO nanoparticles 20-30 nm to ZnO nano- structure via hydrothermal procedure, the first at 70^{o}C, and the second at 90^{o}C, the following steps were obeyed by the two experiments:

The first step was fabricated the hydrothermal system (temperature controller, Teflon lined stainless steel autoclave with volume 100 ml (homemade). For synthesis of nanostructure all row materials were analytical grade .

The Teflon was first cleaned in a diluted HCl (20%) solution for 10 min and then rinsed in de-ionized (DI) water. Subsequently, the substrates were ultrasonically cleaned in an ethanol/acetone (1:1) mixture, then DI water, and dried in air. One gram of ZnO nanoparticles was added to 3,6 or M of NaoH the aqua solution and stirred for twenty minutes, a white suspension appeared, and then the mixture stirred for 1h without heat then the suspension was transferred into a Teflon lined stainless steel autoclave with a volume of 100 ml, the autoclave was sealed and kept at 70 or 90 ^{0}C for 24, 48, and 72 hours .

After that the autoclave cooled down to room temperature. The obtained powder washed several times in ethanol and distilled water and dried at 80 ^{0}C for 30 min then the thick film heated at 500 ^{0}C for 1h to remove residual organic materials.

2.5 Structural and Morphological Measurements

The structure and morphology features of the ZnO nanostructure produced were examined by X-ray diffraction (XRD),field emission scanning electron microscope (FESEM), and atomic force microscope (AFM).

2.5.1 X-Ray Diffraction Investigations

The structure of ZnO nanoparticles were purchased from TECNAN (Spain)(avearge grain size 20-30 nm) and analysis according to the standard testing procedure of Fidena Nanotec,university Alicant and Lurederra centre. Figure 2.5 is showed the XRD of ZnO nanoparticales purchased.

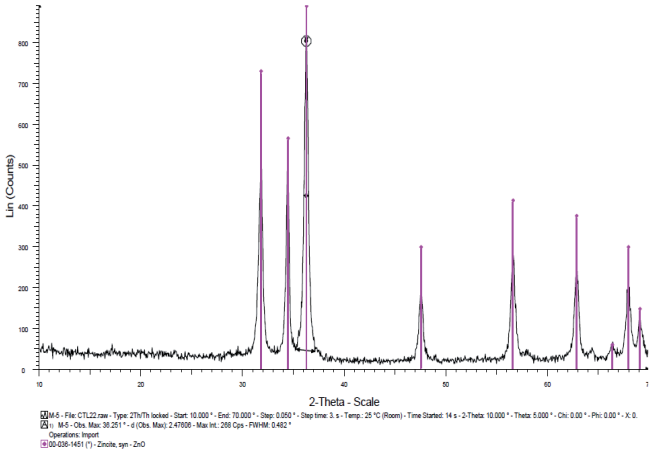

Fig. 2.5 Analysis of XRD for purchased ZnO nanoparticles

The XRD of prepared ZnO nanostructured synthesis by hydrothermal method are carried out by X-ray diffractometers Shimadzu XRD 7000 (Voltage 40 kV 30 mA)maxima Ni filter scan speed 10 deg./min resolution with capper K_α radiation of wavelength λ =1.54 Å was used for measurements ,the scanning angle (2θ)varied in the range $(10\text{-}90)^0$ with speed of 2dgree/min. Figure (2.6) shows the x-ray diffract meter system.

The cell parameters (a and c) are calculated [93] by the relation:

$$d_{hkl} = \frac{a}{\sqrt{\frac{4}{3}\left(h^2+k^2+hk+\frac{l^2a^2}{c^2}\right)}} \qquad (2.\ 1)$$

The crystallite size is calculated using Scherer's equation[93]:

$$D = 0.9\lambda/(\beta cos\theta) \qquad (2.2)$$

Where D: the crystallite size, λ= 1.5406 Å, β: the full width wave maximum (FWHM) and θ: the diffraction angle. Because of the heat treatment process, thick film undergoes a micro strain and dislocations in its structure [94].

The dislocation density is calculated by the equation:

$$\delta = 1/D^2 \qquad (2.3)$$

Fig. 2.6 ***Shimadzu XRD 7000***

2.5.2 Scanning Electron Microscope (SEM)

The electron beam, which typically has an energy ranging from 0.5 keV to 40 keV, is focused by one or two condenser lenses to a spot about 0.4nm to 5 nm in diameter. The beam passes through pairs of scanning coil or pairs of deflector plates in the electron column, typically in the final lens which deflect the beam in the ***x*** and ***y*** axes so that it scans in a raster fashion over a rectangular area of the sample surface. Figure (2.7) .

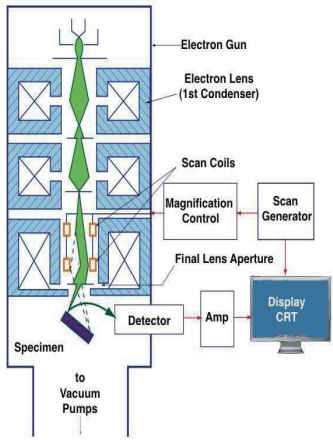

Figure (2.7): A schematic representation of how an SEM works showing all the important components for sample characterization [86].

2.5.3 Atomic Force Microscope (AFM)

Atomic Force Microscope (AFM) measures the interaction force between the tip and surface. The tip may be dragged across the surface, or may vibrate as it moves. The interaction force will depend on the nature of the sample, the probe tip and the distance between them. Using AA3000 Scanning Probe Microscope (atomic scale of resolution 0.26 nm lateral and 0.1nm vertical)with multi functions Atomic Force Microscope (AFM),Scanning Tunnelling Microscope(STM),and Lateral Force Microscope(LFM) Figure (2.8) Shows the SPM AA3000

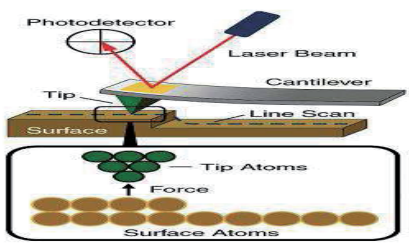

Figure (2.8): Schematic of AFM techniques [89]

2.5.4 Photoluminescence measurements:

Photoluminescence (PL) is an important physical phenomena used to characterize semiconductors which depicts a samples energy structure while possibly revealing other important material features. The transition energy of the samples was measured using the Perkin Elmer Spectrophotometer Luminescence LS 55 equipped with FL Win lab software.

CHAPTER THREE

THE BEHAVIOR OF MANUFACTURING RESULTS

3-1 Introduction

In this chapter, the resultant products were characterized estimated calculations, analyzed and discussed. The chapter consists of the preparation and successfully synthesized of zinc oxide (ZnO) nanostructures from ZnO nanoparticles(1g) with two different sodium hydroxide(NaOH) concentrations (3M , 6M) obtained by hydrothermal method for two different temperatures (70 ^{0}C and 90 ^{0}C) kept for 24 h,48 h and 72 h.

3-2 Structural Characterization results:

3-2-1XRD pattern Analyzing of ZnO nanostructures-prepared with (3M) NaOH at 70 ^{o}C

In order to understand the structural properties of ZnO film samples prepared at different method, the X-ray diffraction study was carried out. X-ray diffraction analysis of ZnO film samples were carried out in the 20-80 range using Cukα radiation. Figure (3-1) shows an XRD pattern of ZnO film samples of ZnO nano structures: (a) arrays as-prepared for 24 h; (b) as-prepared for 48 h and (c) as-prepared for 72 h at 70 ^{o}C plotted in the range 20-80 (2θ) verses intensity having several peaks of zinc oxide indicating the polycrystalline nature and measured inter planer distances agreed with the values reported for ZnO in the literature. The observed peaks matching well with the reported Joint Committee on Powder Diffraction Standards (JCPDS 036–1451)[95] data of Zinc oxide, confirming the polycrystalline nature. The higher peak intensities of an XRD pattern are due to the high crystallinity especially at 72h sample. The increasing in size can be attributed to the agglomeration of particles. The average crystallite size was calculated using Scherrer equation and was estimated to be about 20-30 nm. The sharp diffraction peaks were compared with the peaks according to JCPDS data and found to be

matching and exhibits hexagonal ZnO crystalline structure with lattice constant of a = 3.256 A and c = 5.31, as its reported in JCPDS (36-1451) for bulk ZnO. The diffraction pattern shows strong peak at (100) and (101) plane which confirms that great amount of nanostructure has aligned on the substrate and grown with orientation along the c axis. However no diffraction peak from elemental Zn metal or other impurities were not found in the samples. The diffraction patterns reveal good crystalline quality without any appreciable changes from pure ZnO films and are polycrystalline with a hexagonal wurtzite structure. The corresponding reflecting planes are (100), (002), (101), (102), (110), (103) and (112) respectively. The XRD patterns of all the samples indicated enhanced intensities for the peak corresponding to (101) plane, indicating preferred orientation along the c-axis. The lattice parameters were found close to the typical values. The higher dislocation density was occur forward lattice plane (101) have (3.51 x 10^{15}, 11.9 x 10^{15}, and 2.8 x 10^{15}) line^2/m^2 for reaction times 24, 48 and 72 h respectively The structural parameters estimated and illustrated in table 3.1.

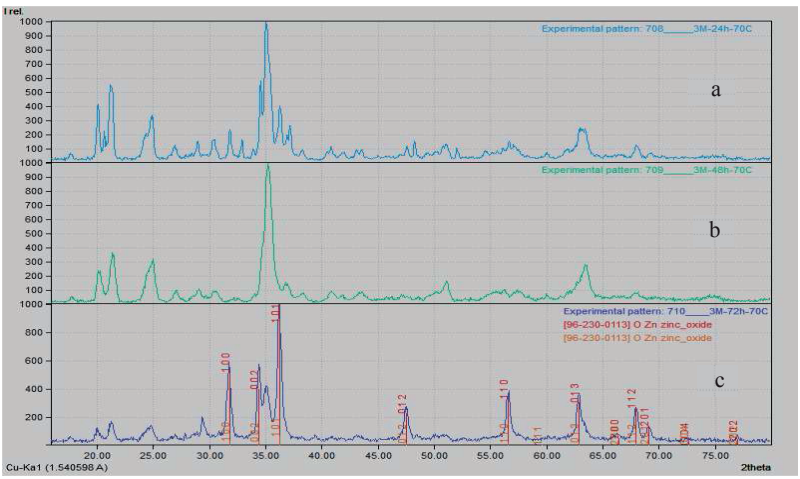

Fig 3.1 XRD pattern of ZnO nano structures: (a) arrays as-prepared for 24h (b) as-prepared for 48 h and (c) as-prepared for 72 h at 70 ^{o}C

Table 3.1 the estimated structural parameters (a = 3.228 A°, c = 5.272 A°) at 70 °C

3M (NaOH) 24h						
Lattice plane	2θ (Deg)	FWHM (radian)	Int.%	d(h k l) (A°)	Grain size (nm)	Dislocation density δ x10^{15}(line^2/m^2)
(100)	31.838	0.364	18	2.808	21.3795	2.18
(002)	34.920	0.429	100	2.567	18.2869	2.99
(101)	36.271	0.466	35	2.475	16.8987	3.50
(102)	47.560	0.360	8	1.910	22.7155	1.93
(110)	56.570	0.320	12	1.626	26.5549	1.41
(103)	63.100	0.941	23	1.472	9.3312	11.4
(112)	67.930	0.499	8	1.379	18.0797	3.05
	3M (NaOH) 48h					
Lattice plane	2θ (Deg)	FWHM (radian)	Int.%	d(h k l) (A°)	Grain size (nm)	Dislocation density δ x10^{15}(line^2/m^2)
(100)	30.520	0.630	7	2.927	12.3130	6.59
(002)	34.990	0.782	100	2.562	10.0340	9.93
(101)	36.780	0.860	12	2.442	9.1701	11.8
(102)	47.230	0.780	3	1.923	10.4708	9.12
(110)	56.170	0.620	6	1.636	13.6802	5.34
(103)	62.670	0.850	10	1.481	10.3065	9.41
(112)	67.900	0.637	40	1.379	14.1604	4.98
	3M (NaOH) 72h					
Lattice plane	2θ (Deg)	FWHM (radian)	Int.%	d(h k l) (A°)	Grain size (nm)	Dislocation density δ x10^{15}(line^2/m^2)
(100)	31.837	0.416	52	2.809	18.7070	2.85
(002)	34.514	0.390	56	2.597	20.0933	2.47
(101)	36.314	0.417	100	2.472	18.8867	2.80
(102)	47.598	0.401	25	1.909	20.3959	2.40
(110)	56.650	0.404	37	1.623	21.0415	2.25
(103)	62.913	0.385	36	1.476	22.7840	1.92
(112)	68.005	0.373	27	1.377	24.1977	1.70

3-2-2 XRD pattern Analyzing of ZnO nanostructures-prepared with (3M) NaOH at 90 °C

Figure 3.2 shows the XRD patterns recorded in the range of 20–80◦ with a scanning step of 0.02◦ of ZnO nano structures prepared from 1g ZnO nanoparticles with 3M NaOH concentration at 90 °C for 24 h ,48 h and 72 h .

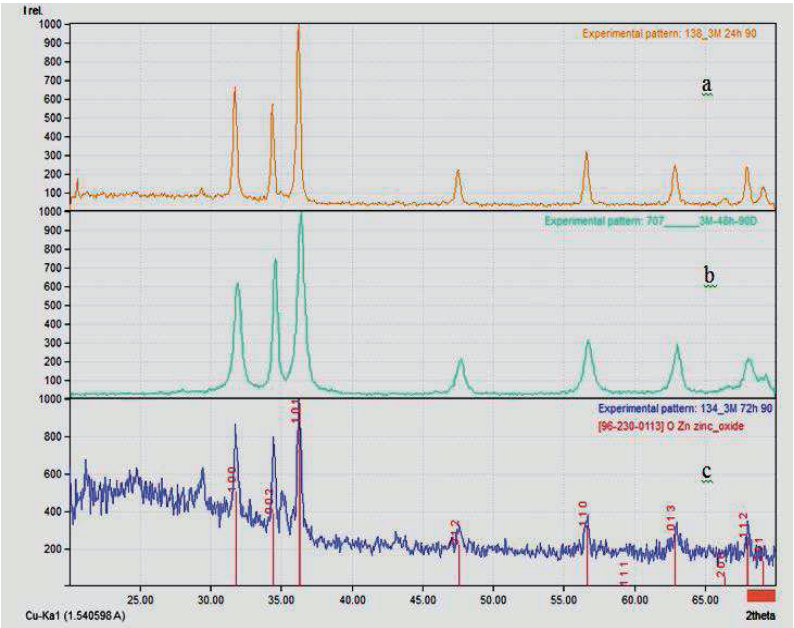

Fig. 3.2 XRD pattern of ZnO nano rods: (a) arrays as-prepared at 90 °C for 24h (b) as-prepared at 90 °C for 48 h; (c) as-prepared at 90 °C for 72 h

The data are in agreement with the Joint Committee on Powder Diffraction Standards (JCPDS) card for ZnO the patterns show the strongest detected (h k l) peaks are at 2θ values of 31.72°, 34.38°, 36.21°, 47.49°, 56.566, 62.83°, and 67.930° for reaction time 24 h and for 48 h ware 31.92°, 34.57°, 36.39° , 47.67°, 56.70°, 62.97°, and 68.06° finally for reaction time 72 h were 31.83°, 34.51°, 36.31°, 47.59°, 56.65°, 62.91° and 68.00° corresponding to the following lattice planes: (1 0 0), (0 0 2), (1 0 1), (1 0 2), (1 1 0), (1 0 3),and (112) respectively(see Table 3.2). From the diffraction pattern it's obvious that the growth is dominated in these

directions and these diffraction peaks can be assigned to the wurtzite hexagonal-shaped ZnO. The lattice constants a and c were determined as a = 3.228 **Å**, c = 5.272 **Å.** .The estimated structure parameters was found closed to typical results also the dislocation density was estimated and depend on the reaction conditions such as the growth reaction time and temperature[96]. The higher dislocation density was occur forward lattice plane (110),(112), and(100) have (1.53 x 10^{15}, 5.93 x 10^{15}, and 1.33 x 10^{15}) line^2/m^2 for reaction times 24, 48 and 72 h respectively.

Table 3.2The estimated structural parameters (a = 3.228 Å, c = 5.272 Å) 3M (NaOH)at 90 ^{o}C.

3M (NaOH) 24 h						
Lattice plane	2θ (Deg)	FWHM (radian)	Int.%	d(h k l) (A°)	Grain size (nm)	Dislocation density δ x10^{15}(line^2/m^2)
(100)	31.728	0.297	63	2.818	26.195	1.45
(002)	34.389	0.240	57	2.606	32.64	0.93
(101)	36.211	0.295	100	2.479	26.68	1.40
(102)	47.490	0.320	19	1.913	25.54	1.53
(110)	56.566	0.290	32	1.626	29.30	1.16
(103)	62.838	0.302	25	1.478	29.342	1.18
(112)	67.930	0.250	25	1.379	36.08	0.76
	3M (NaOH) 48 h					
Lattice plane	2θ (Deg)	FWHM (radian)	Int.%	d(h k l) (A°)	Grain size (nm)	Dislocation density δ x10^{15}(line^2/m^2)
(100)	31.920	0.570	60	2.801	13.6556	5.36
(002)	34.570	0.395	70	2.593	19.8420	2.53
(101)	36.390	0.558	100	2.467	14.1173	5.01
(102)	47.670	0.581	20	1.906	14.0809	5.04
(110)	56.700	0.607	30	1.622	14.0079	5.09
(103)	62.970	0.590	26	1.475	14.8721	4.52
(112)	68.060	0.696	18	1.376	12.97	5.94
	3M (NaOH) 72 h					
Lattice plane	2θ (Deg)	FWHM (radian)	Int.%	d(h k l) (A°)	Grain size (nm)	Dislocation density δ x10^{15}(line^2/m^2)
(100)	31.837	0.284	67	2.817	27.3952	1.33

(002)	34.514	0.283	74	2.601	27.6563	1.30
(101)	36.314	0.310	100	2.477	25.3996	1.55
(102)	47.598	0.238	22	1.911	34.3569	0.84
(110)	56.650	0.264	33	1.626	32.1878	0.96
(103)	62.913	0.261	26	1.477	33.6013	0.88
(112)	68.005	0.331	14	1.377	27.2705	1.34

3-2-3 XRD pattern Analyzing of ZnO nanostructures-prepared with (6M) NaOH at 70 ^{o}C

Patterns recorded of XRD in the range of 10–70◦ with a scanning step of 0.02◦ of ZnO nanostructures prepared from 1g ZnO nanoparticles with 6M NaOH concentration at 70 ^{o}C for 24 h ,48 h and 72 h are showed in figure 3.3 .

The patterns show the strongest detected (h k l) of major peaks at 2θ values of 31.96°, 34.61°,and 36.44°,are founded corresponding to the lattice planes (1 0 0), (0 0 2),and (1 0 1) respectively for reaction time 24 h and major peaks are at 2θ values of for 48 h ware 32.03°, 34.730°, and 36.39°, corresponding to the lattice planes (1 0 0), (0 0 2),and (1 0 1) respectively. Finally for reaction time 72 h were appeared the new growth at 2θ value 21.44°,and disappeared growth lattice plane 31.96°obvious that the growth is dominated in these new directions structure forward new lattice plane.

These directions and these diffraction peaks cannot be assigned to the wurtzite hexagonal-shaped ZnO. The dislocation density was proportion with the peak relative intensity so that observed for 100% relative intensity has a maximum value for this process conditions. The structural parameters estimated and illustrated in table 3.3.

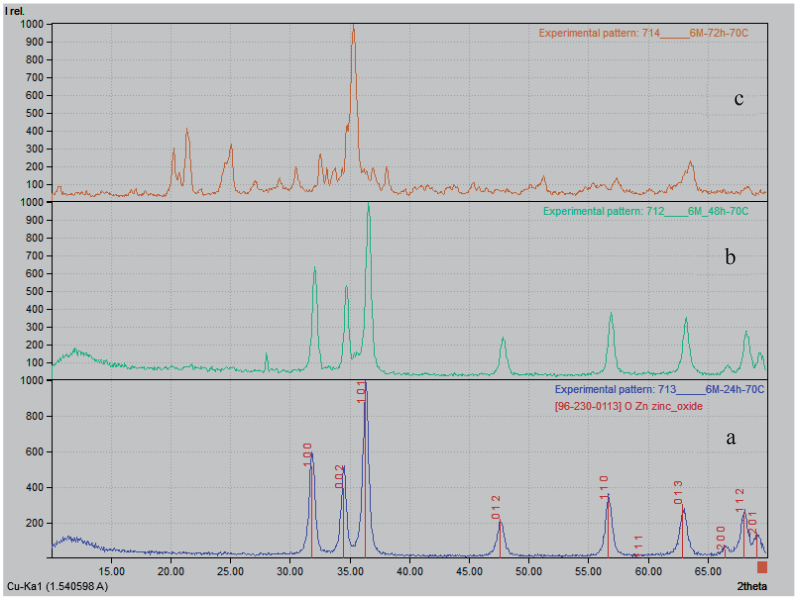

Fig. 3.3 XRD pattern of ZnO nano structured prepared from 1g of ZnO with 6M NaOH at 70 ^{o}C: (a) arrays as-prepared for 24h (b) as-prepared at for 48 h; (c) as-prepared at for 72 h

Table 3.3 the estimated structural parameters of major peaks (a = 3.228 Å , c = 5.272 Å) 6M (NaOH)at 70 ^{o}C.

6M 24 h 70 ^{o}c							
Peak No.	Lattice plane	2θ (Deg)	FWHM (radian)	Int.%	d(h k l) (A°)	Grain size (nm)	Dislocation density δ x10^{15} (line^{2} /m^{2})
1	(100)	31.960	0.531	61	2.798	46.601	4.65
2	(002)	34.619	0.484	50	2.589	61.955	3.8
3	(101)	36.445	0.551	100	2.463	42.989	4.89
6M 48 h 70 ^{o}c							
Peak No.	Lattice plane	2θ (Deg)	FWHM (radian)	Int.%	d(h k l) (A°)	Grain size (nm)	Dislocation density δ x1015(line2/m2)
1	(100)	32.030	0.455	61	2.792	17.1	3.415
2	(002)	34.730	0.431	50	2.581	18.1	3.021
3	(101)	36.550	0.509	100	2.456	15.4	4.171
6M 72 h 70 ^{o}c							
Peak No-	Lattice plane	2θ (Deg)	FWHM (radian)	Int.%	d(h k l) (A°)	Grain size (nm)	Dislocation density δ x10^{15} (line^{2} /m^{2})
1	(100)	21.440	0.494	40	4.141	15.4	4.20
2	(002)	34.680	0.347	29	2.585	22.5	1.95
3	(101)	35.306	0.606	100	2.540	12.9	5.95

3-2-4 XRD pattern Analyzing of ZnO nanostructures-prepared with (6M) NaOH at 90 ^{o}C

Patterns recorded of XRD in the range of 20–80◦ with a scanning step of 0.02◦ of ZnO nanostructures, at 90 ^{o}C for 24 h ,48 h and 72 h are showed in figure 3.4 .

From the diffraction pattern it's obvious that the growth is dominated in these directions and these diffraction peaks can be assigned to the wurtzite hexagonal-shaped ZnO was consummated only the sample prepared with the growth reaction time 48h, and have major peaks at 2θ values of 31.62°, 34.28°, and 36.11°, are which corresponding to the lattice planes (1 0 0), (0 0 2), and (1 0 1) respectively (fig 3.4 b). For reaction times 24h and 72 h were appeared the new growth at 2θ value 21.16°,and 21.17° respectively, and shifting growth lattice plane the growth is dominated in these new directions structure forward new lattice plane see fig 3.4(a and c), These directions and these diffraction peaks cannot be assigned to the wurtzite hexagonal-shaped ZnO. The higher dislocation density was occur forward lattice plane (101) have (1.01 x 10^{15}, 2.89 x 10^{15}, and 0.936 x 10^{15}) line^{2}/m^{2} for reaction times 24, 48 and 72 h respectively. The structural parameters estimated and illustrated in table 3.4.

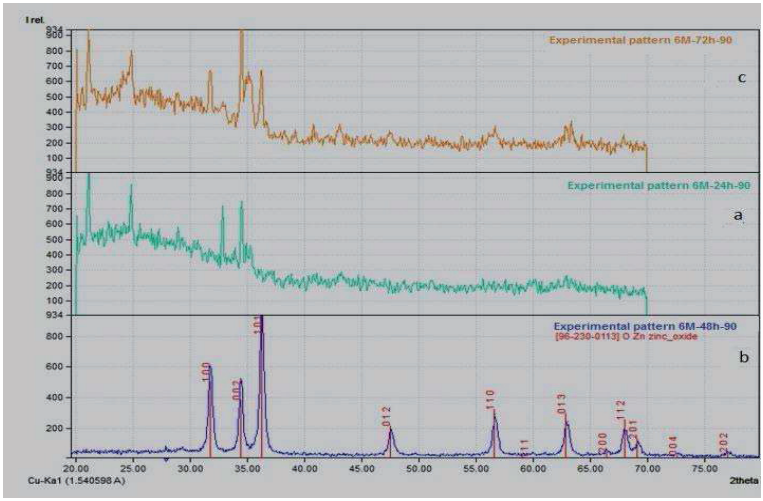

Fig. 3.4 XRD pattern of ZnO nano structured prepared from 1g of ZnO with 6M NaOH at 90 ^{o}C: (a) arrays as-prepared for 24h (b) as-prepared at for 48 h; (c) as-prepared at for 72 h

Table 3.4 the estimated structural parameters of major peaks (a = 3.228 Å, c = 5.272 Å) 6M (NaOH) at 90 ^{o}C

6M 24 h 90 ^{o}c							
Peak No.	Lattice plane	2θ (Deg)	FWHM (radian)	Int.%	d(h k l) (A°)	Grain size (nm)	Dislocation density δ x10^{15} (line /m^{2})
1	(100)	21.168	0.240	100	4.194	31.7	0.993
2	(002)	32.860	0.212	80	2.723	36.8	0.738
3	(101)	34.520	0.250	87	2.596	31.3	1.01
6M 48 h 90 ^{o}c							
Peak No.	Lattice plane	2θ (Deg)	FWHM (radian)	Int.%	d(h k l) (A°)	Grain size (nm)	Dislocation density δ x1015(line /m^{2})
1	(100)	31.620	0.425	40	2.827	18.30	2.98
2	(002)	34.280	0.368	29	2.614	21.2	2.208
3	(101)	36.110	0.421	100	2.485	18.6	2.86
6M 72 h 90 ^{o}c							
Peak No.	Lattice plane	2θ (Deg)	FWHM (radian)	Int.%	d(h k l) (A°)	Grain size (nm)	Dislocation density δ x10^{15} (line /m^{2})
1	(100)	21.176	0.242	67	4.192	31.46	0.101
2	(002)	34.521	0.228	100	2.596	34.38	0.846
3	(101)	36.240	0.241	61	2.477	32.66	0.936

3-3 Surface Morphology

3-3-1 Atomic Force Microscope (AFM) results:

3-3-1-1 Atomic Force Microscope (AFM) for ZnO nanostructures-prepared with (3M) NaOH at 70 ^{o}C

Good information about the topography of the surface of the film gives us by the Atomic Force microscope technique. It is known that the surface properties of the transparent conducting oxide films influence their optical and electrical properties which are important parameters for applications in optoelectronic devices; in principle, the increase in surface roughness of the films effects the optical properties of the films .Therefore, it is very important to investigate the surface morphology of the films. The average of grain size on the surface is found by granularity Cumulating distribution chart to be 73.41 nm for the sample as prepared for 24 h as shown in figure 3.5.

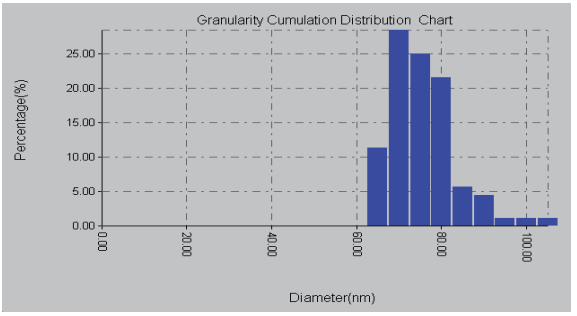

Fig 3.5: Shows the granularity cumulating distribution for nanostructure prepared for 24 h

Fig 3.6 Shows the granularity cumulating distribution as appeared of 99 nm for the nanostructured prepared for 48h.

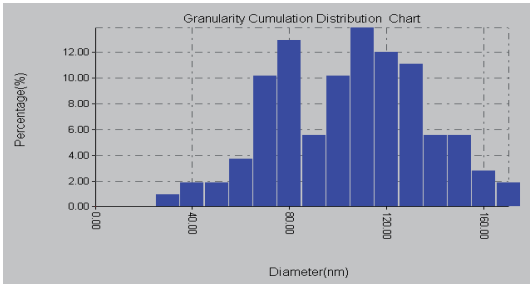

Fig 3.6 Shows the granularity cumulating distribution for nanostructure prepared for 48 h

The nanostructured prepared for 72 h have granularity cumulating distribution shows in fig 3.7 which refer to the average grain size about 76 nm Figure3.8 show the AFM pictures morphology of the surface of the ZnO thick film in three dimensions of the samples prepared of ZnO (1g) with 3M concentration of NaOH at 70 ^{0}C for 24 ,48, and 72 h.

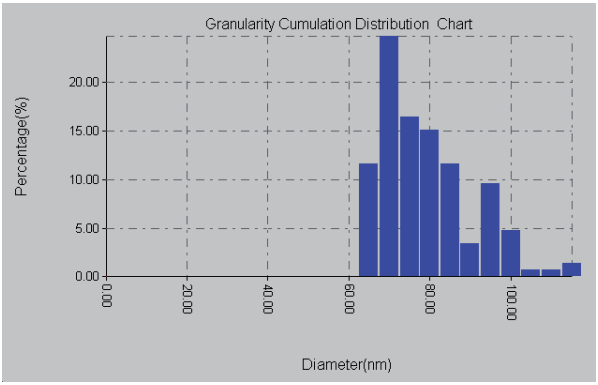

Fig 3.7: Shows the granularity cumulating distribution for ZnO nanostructure prepared for 72 h

.

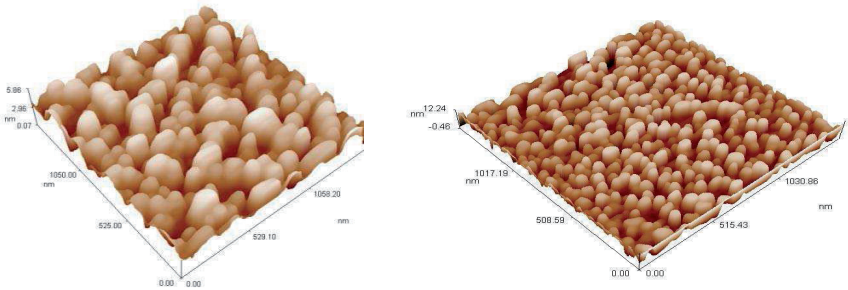

a b

Fig. 3.8 AFM images of the ZnO nanostructure with NaOH(3M) aqueous at 70 °c for (A) 24 h, (B)48 h and (C) 72

The roughness of the surface (SA), and peak to peak for the prepared films are showed in figure 3.9 refer to the best preparation was found that at time reaction 72 h where its observed a high ratio of the surface grain lies in the range nanostructured for sensors application

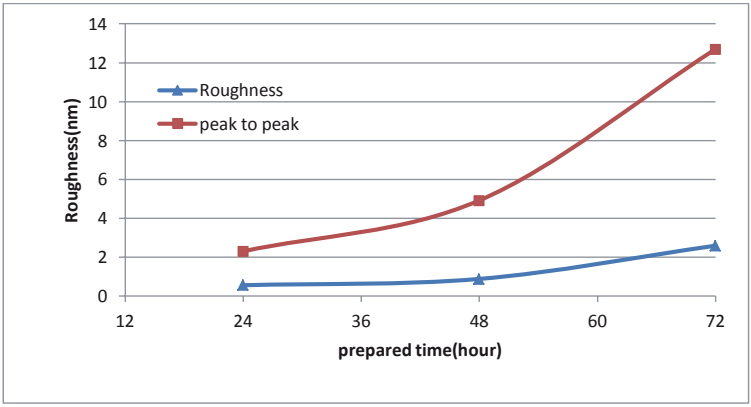

Fig. 3.9: Shows the surface roughness of the ZnO nanostructured with 3M NaOH at 70 °C

The best results at 72 h because of the interaction between the NaOH aqueous and ZnO nanoparticles, due to the presence of sufficient temperature and reaction time in the form that gave the opportunity to the formation of the level of growth consequent that interpreted the internal pressure is higher than the external pressure of the nano structured growth material formed especially since results showed the presence of nanostructured (nanotubes).

3-3-1-2 AFM for ZnO nanostructures-prepared with (3M) NaOH at 90 °C

The average of grain size on the surface is found by granularity Cumulating distribution chart to be 86 nm for the sample as prepared for 24 h as shown in figure 3.10

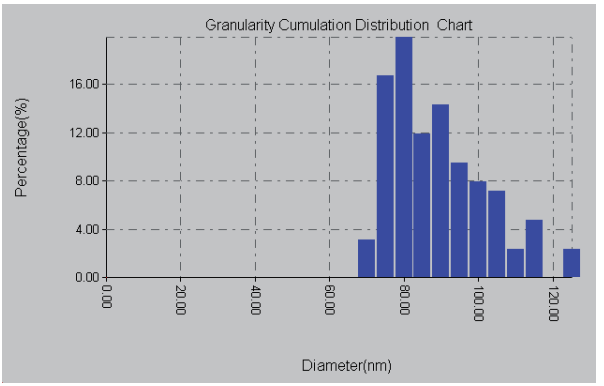

Fig 3.10 shows the granularity cumulating distribution for nanostructure prepared for 24 h

The average of grain size is 75 nm for the sample as prepared for 48 h as shown in figure 3.11

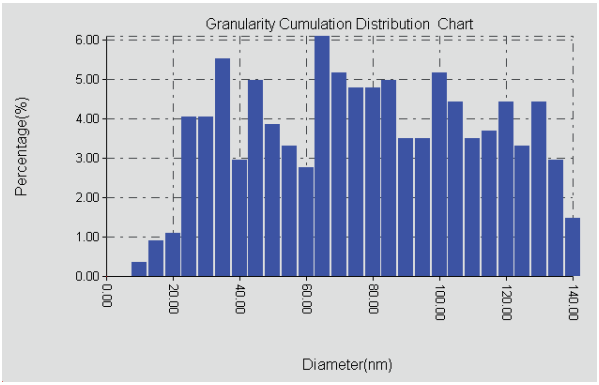

Fig 3.11 :Shows the granularity cumulating distribution for nanostructure prepared for 48 h

By the chart the average of grain size to be 77 nm for the sample as prepared for 72h as shown in figure 3.12

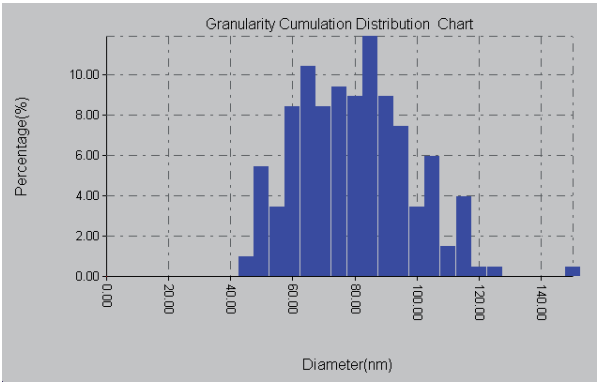

Fig 3.12 shows the granularity cumulating distribution for nanostructure prepared for 72 h

Figure 3.13 shows the AFM pictures morphology of the surface of the ZnO thick film in three dimensions of the samples prepared at 90 ^{o}C for 24 h, 48 h, and 72 h. The SA and peak to peak for the prepared films are shown in figure 3.14. The cumulating distribution report of scan probe microscope (SPM) for the grains diameters of the sample indicate high percentage less than 100 nm.

Fig. 3.13 AFM images of the ZnO nano rods hydrothermally grown with (3M) NaOH aqueous at 90 ^{o}c for (a) 24 h, (b)48 h and (c) 72 h

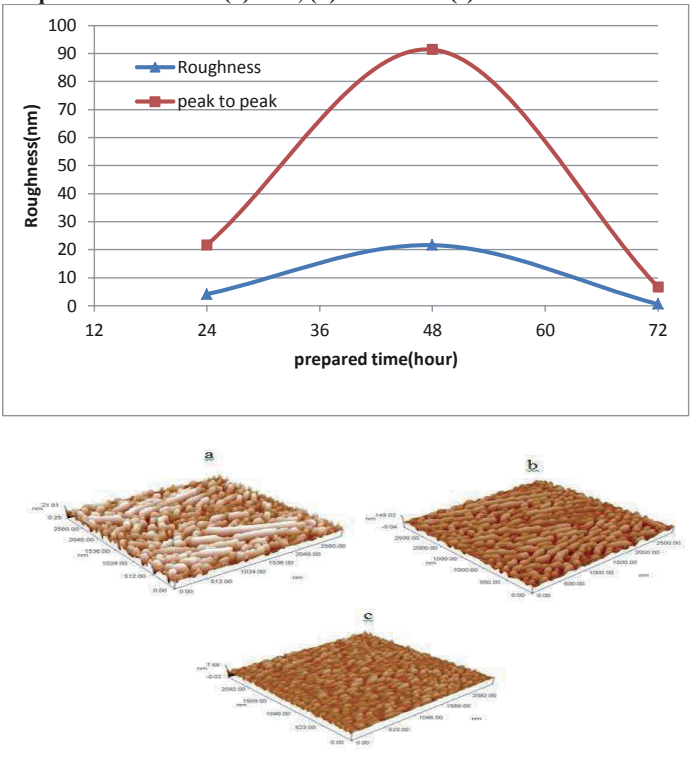

Fig. 3.14 shows the surface roughness of the ZnO nanostructured prepared of ZnO (1g) nanoparticles with NaOH (3M) at 90 ^{o}C

The best results was found at 48 h due to of the interaction between the NaOH aqueous and ZnO nanoparticles, the reason is that the presence of

sufficient temperature and reaction time in the form that gave the opportunity to the formation of the level of growth consequent that interpreted the external pressure is higher than the internal pressure of the material formed especially since results showed the presence of nanostructured.

3-3-1-3 Atomic Force Microscope (AFM) for ZnO nanostructures-prepared with NaOH (6M) at 70°C

The average of grain size on the surface is found by granularity Cumulating distribution chart to be 113 nm for the sample as prepared for 24 h as shown in figure 3.15.

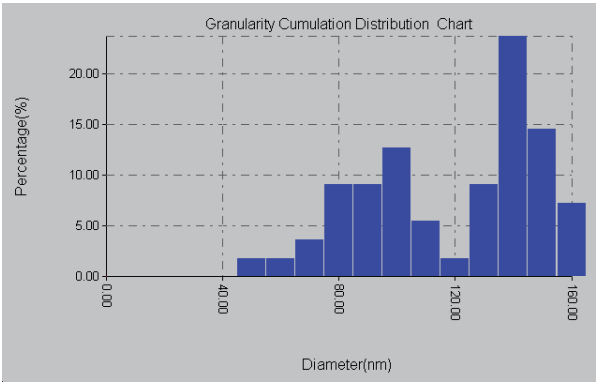

Fig 3.15 shows the granularity cumulating distribution for nanostructure prepared for 24 h

The average of grain size on the surface is found by granularity Cumulating distribution chart to be 80 nm for the sample as prepared for 48 h as shown in figure 3.16.

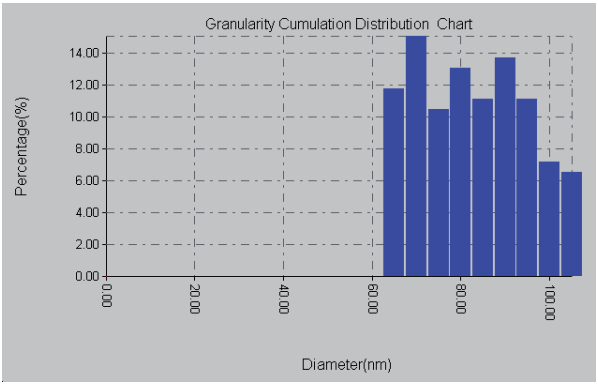

Fig 3.16 shows the granularity cumulating distribution for nanostructure prepared for 48 h

The average of grain size on the surface is found by granularity Cumulating distribution chart to be 97 nm for the sample as prepared for 72 h as shown in figure 3.17.

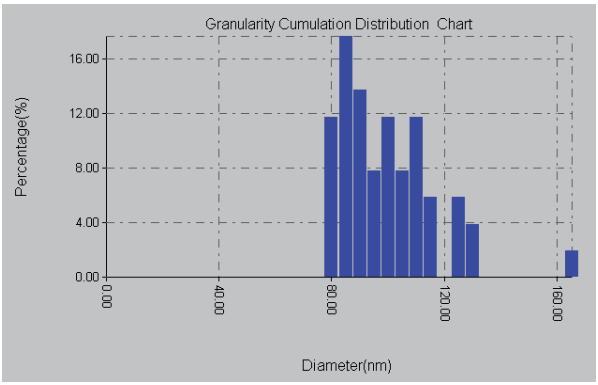

Fig 3.17 shows the granularity cumulating distribution for nanostructure prepared for 72 h

Figure 3.18 shows the AFM pictures morphology of the surface of the ZnO thick film in three dimensions of the samples prepared at 70 ^{o}C for 24 h, 48 h, and 72 h. The SA and peak to peak for the prepared films are showing in figure 3.19. The cumulating distribution report of scan probe

microscope (SPM) for the grains diameters of the sample indicate high percentage less than 100 nm excepted the sample prepare for 24 h.

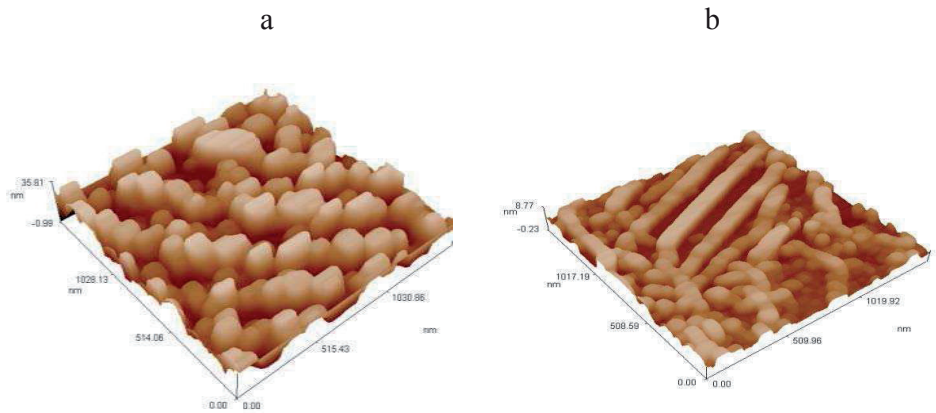

Fig. 3.18 AFM images of the ZnO nanostructure with NaOH(3M) aqueous at 70 ^{o}c for (a) 24 h, (b)48 h and (c) 72 h

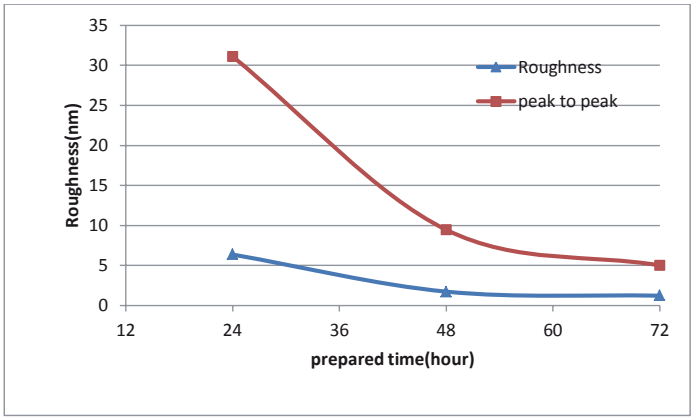

Fig. 3.19 shows the surface roughness of the ZnO nanostructured prepared of ZnO (1g) nanoparticles with NaOH (6M) at 70 ^{o}C .

At first glance it seems that the best result was a sample that prepared for 24 h, but it cannot be considered as the optimal outcome due to the fact that structured which is to be nano structured (more than 100nm) because the features of micro dimension balk is different completely with nano dimensions therefore it is to be the best sample recorded at the prepared condition at 48 h .

3-3-1-4 Atomic Force Microscope (AFM) for ZnO nanostructures-prepared with NaOH (6M) at 90 ^{o}C

The average of grain size on the surface is found by granularity Cumulating distribution chart to be 82 nm for the sample as prepared for 24 h as shown in figure 3.20

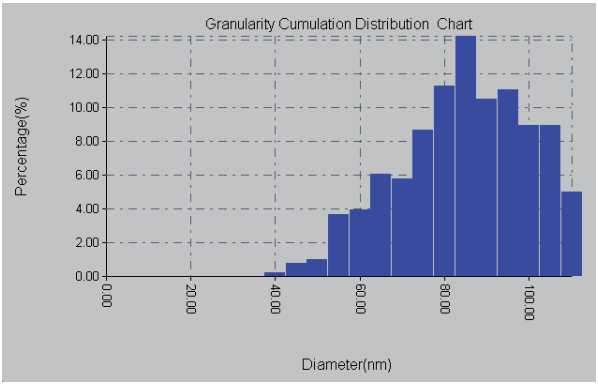

Fig. 3.20 shows the granularity cumulating distribution for nanostructure prepared for 24 h

The average of grain size on the surface is found by granularity Cumulating distribution chart to be 86 nm for the sample as prepared for 48 h as shown in figure 3.21.

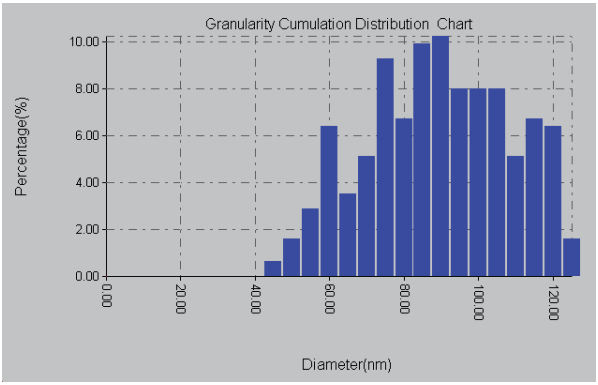

Fig. 3.21shows the granularity cumulating distribution for nanostructure prepared for 48 h

The average of grain size on the surface is found by granularity Cumulating distribution chart to be 100 nm for the sample as prepared for 72 h as shown in figure 3.22.

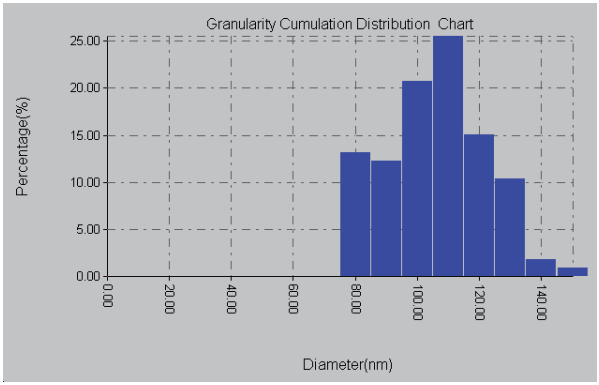

Fig.3.22 shows the granularity cumulating distribution for nanostructure prepared for 72 h.

Figure 3.23 shows the AFM pictures morphology of the surface of the ZnO thick film in three dimensions of the samples prepared at 70 ^{o}C for 24 h, 48 h, and 72 h.

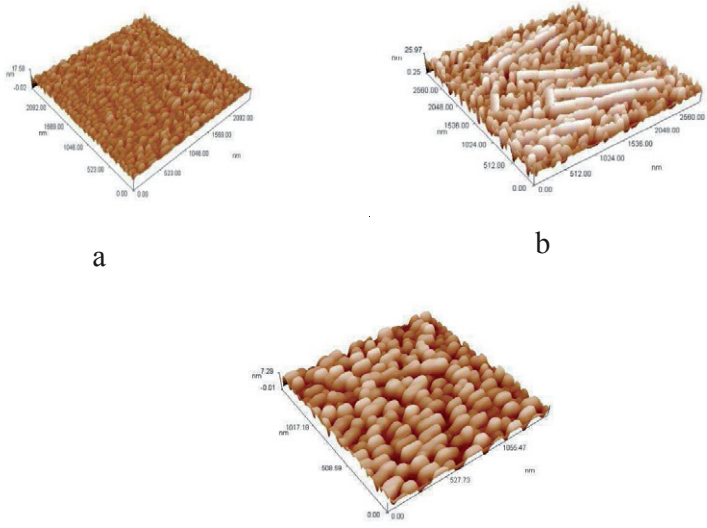

Fig. 3.23 AFM images of the ZnO nanostructure with NaOH(3M) aqueous at 90 ^{o}c for (A) 24 h, (B)48 h and (C) 72 h

The roughness of the surface SA and peak to peak for the prepared films are showing in figure 3.24. The cumulating distribution report of scan probe microscope (SPM) for the grains diameters of the sample indicate high percentage less than 100 nm.

The surface roughness of the ZnO nanostructured prepared of ZnO (1g) nanoparticles with NaOH (6M) at 90 ^{o}C as showing in the Figure 3.24.

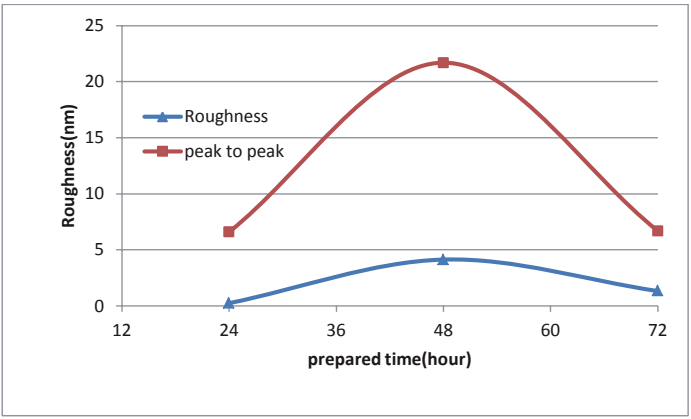

Fig. 3.24 shows the surface roughness of the ZnO nanostructured prepared of ZnO (1g) nanoparticles with NaOH (6M) at 90 ^{o}C.

The best results were found as the 48 h because of the interaction between the NaOH aqueous and ZnO nanoparticles, the reason is that the presence of sufficient temperature and reaction time in the form that gave the opportunity to the formation of the level of growth consequent that interpreted the external pressure is higher than the internal pressure of the material formed especially since results showed the presence of nanostructured.

3-3-2 Scan Electron Microscopic and Field Emission Scan Electron Microscopic (FE-SEM) results :

The morphology of ZnO nanostructures prepared by hydrothermal method were characterizes by scan electron microscope and field emission scan electron microscope (FE-SEM) images. In Hydrothermal method, the reaction time, pressure, concentration of solvent, pH of the solution, and temperature are five significant parameters that are affected on the size and the shape of the hydrothermally synthesized. The growth temperature and time needs to (with solvent concentration) be carefully controlled in order to obtain desired ZnO nanostructures. It has been observed that the change of the growth temperature and time contributes to a large variation on the morphology of nanostructures.

3-3-2-1 Scan Electron Microscopic (SEM) and Field Emission Scan Electron Microscopic (FE-SEM) for ZnO nanostructures-prepared with (3M) NaOH at 70 ^{o}C

The FE-SEM over view image of ZnO nanostructures of 1 g ZnO nanoparticles and 3M of NaOH with different growth time 24, 48 and 72hour are shown in figures 3.25, 3.26 and 3.27 respectively at 70 ^{o}C. It can be clearly seen the images from figure 3.25 (growth time reaction 24h) that the heterogeneous structured multilayers nano plates and nanoparticles it's clear that the grain size about 74nm with the nano scale for width the plates this result is comfortable and agreement with the AFM results (fig 3.5 and fig 3.8) and agreement with the XRD behavior (fig 3.1a).

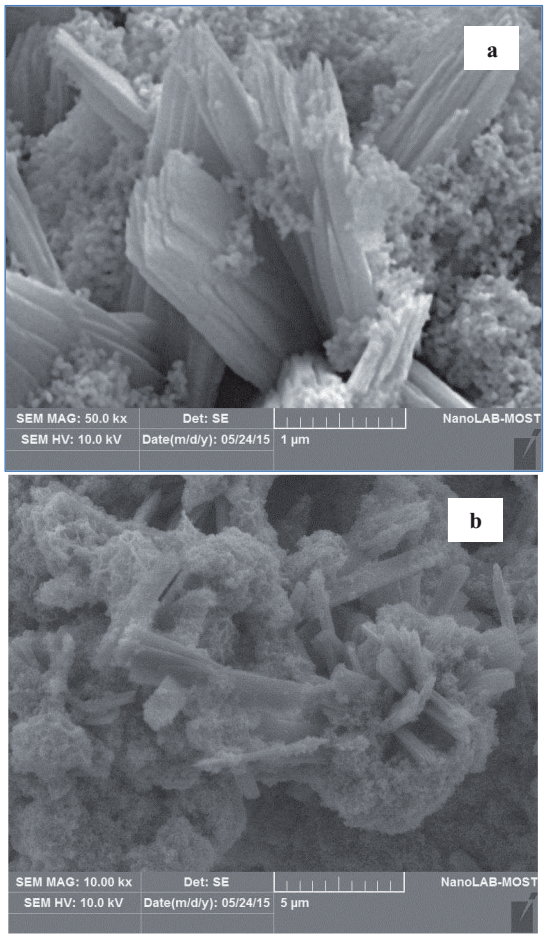

Fig 3.25: a ,b shows growth of the ZnO structured preparation from 1g ZnO nanoparticles with 3M NaOH at 70 ^{0}C for 24h appeared heterogeneous structured (multilayer nano plates with nanoparticles)

Figure 3.26 shows the growth reaction time 48h it can be clearly seen from the initially ZnO nanotube growth with grain size about 90nm.the growth reaction time and pressure indicated inadequate for nanotubes growth .The FE-SEM results is agreement with AFM (fig 3.6 and 3.8 B)and XRD behavior (fig 3.1 b).

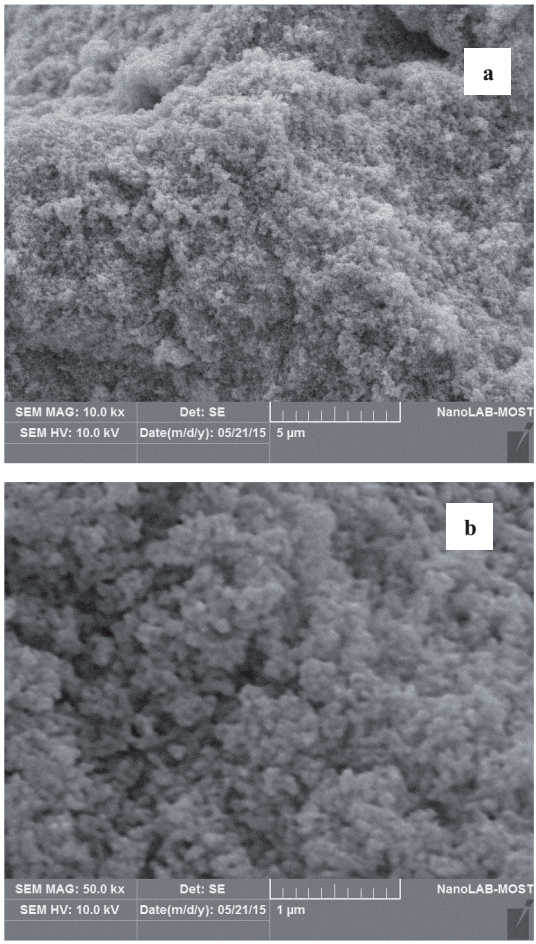

Fig 3.26:a,b Shows growth of the ZnO structured preparation 1g ZnO nanoparticles with 3M NaOH at 70 ^{o}C for 48h appeared initially nanotubes growth

Fig. 3.27Nanotubes structured of ZnO grown are prepared from 1g ZnO nanoparticles with 3M NaOH at 70 ^{o}C for reaction time 72h are appeared with wall thickness are founded about 10- 30 nm and average outer diameters about 70 -150nm and inner diameters are founded about 60-120nm. the results are pointing to the inner pressure is greater than outer pressure of structure grown for this process ,it was indicated the

agreement with the interpreted nanotube formation, and that compatible with AFM resulting (fig3.7 and fig 3.8 C).The reaction time, temperature and concentration of NaOH resulting hexagonal ZnO nanotube crystalline structure its reported in JCPDS(36-1451)the diffraction pattern shows strong peak at (100) and (101) plane which confirms that great amount of nanostructure has aligned and grown with orientation along the c axis this result is agreement with XRD behavior (fig 3.1 c) .

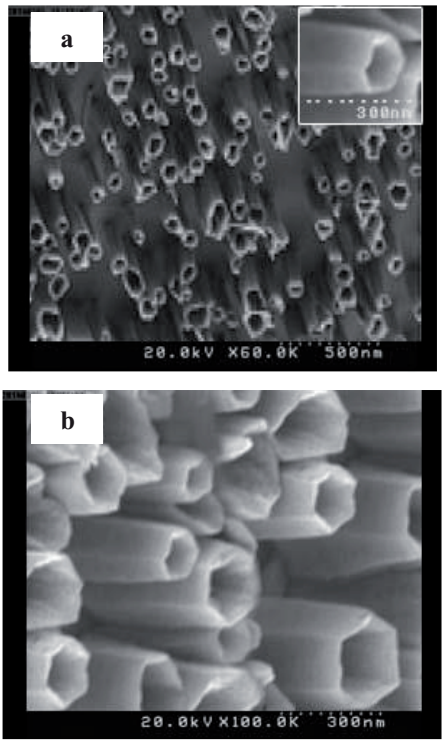

Fig 3.27:a,b show Nanotubes structured of ZnO growth are prepared from 1g ZnO nanoparticles with 3M NaOH at 70 ^{o}C for reaction time 72h

3-3-2-2Scan Electron Microscopic and Field Emission Scan Electron Microscopic (FE-SEM) **for** *ZnO nanostructures-prepared with (3M) NaOH at 90 ^{o}C*

The FE-SEM over view image of ZnO nanostructures prepared of 1 g ZnO nanoparticles and 3M of NaOH with different growth time 24, 48 and 72 hour are shown in figures 3.28, 3.29 and 3.30 respectively at 90 ^{o}C. Nanobelts structures of ZnO growth for reaction time 24h are appeared, with wall thickness about 40 nm and average width 300nm this result are clearly showed as FE-SEM images in figure 3.28**.**

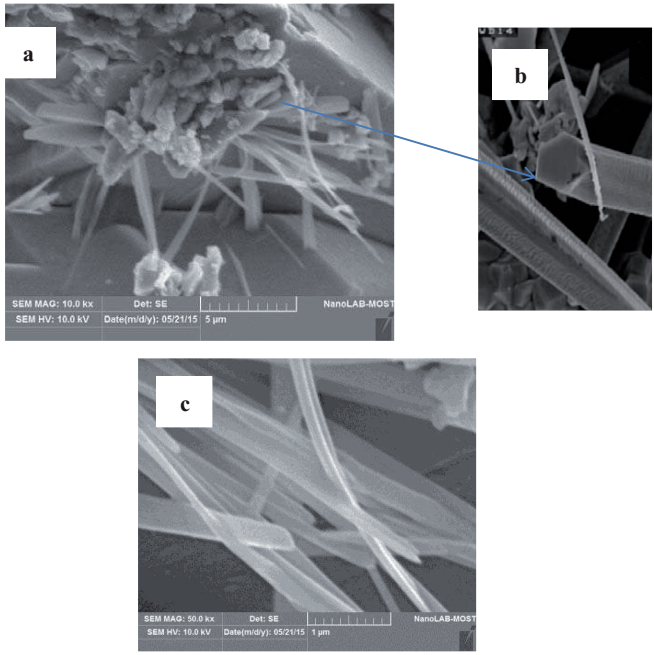

Fig 3.28:a,b and c shows growth of the ZnO growth are prepared from 1g ZnO nanoparticles with 3M NaOH at 90 ^{o}C for 24h appeared the Nanobelts structures

Figure 3.29 shows the images growth reaction time 48h it can be clearly seen from the nanorods structured of ZnO growth with average diameters about 75nm. The results are pointing to the inner pressure is less than

outer pressure of structure grown for this process, it was indicated the agreement with the interpreted nanorods formation. The FE-SEM images are agreement with AFM resulting (fig 3.11 and 3.13b) and XRD behavior (fig 3.2 b).

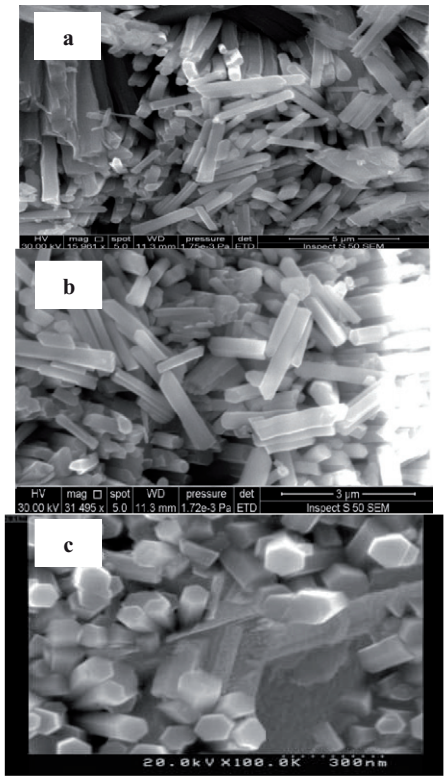

Fig 3.29:a,b and c shows growth of the ZnO are prepared from 1g ZnO nanoparticles with 3M NaOH at 90 ^{o}C for48 h appeared the nano rods structures

It can be clearly seen from the flowerlike structured of ZnO growth for reaction time 72h with average diameters about 77nm (Figure 3.30). The growth results are pointing to non-homogenously grown for polycrystalline may be the pressure and reaction time ar more effective parameters to formation this structure. The FE-SEM images are

agreement with AFM resulting (fig 3.12 and 3.13c) and XRD behavior (fig 3.2 c).

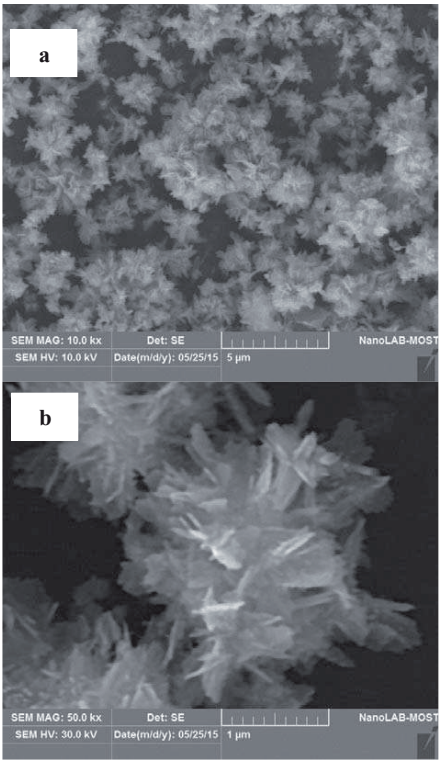

Fig 3.30:a,b shows growth images of the ZnO are prepared from 1g ZnO nanoparticles with 3M NaOH at 90 ^{o}C for 72 h appeared nano flowerlike structures

3-3-2-3Scan Electron Microscopic (SEM) and Field Emission Scan Electron Microscopic (FE-SEM)) for ZnO nanostructures-prepared with (6M) NaOH at 70 ^{o}C

The FE-SEM over view image of ZnO nanostructures of 1 g ZnO nanoparticles and 6M of NaOH with different growth time 24, 48 and 72hour are shown in figures 3.31, 3.32 and 3.33 respectively at 70 ^{o}C.

Figure 3.31 are showing the FE-SEM images ZnO nano structure prepared from 1g ZnO nanoparticles with 6M NaOH at 70 ^{o}C for 24h. Images are showed the lettuce leaf structure with average diameter 113nm and thickness about 20 nm. This structure is very important for solar cells applications and bio sensors .The conclusion of mechanical grown which depends of the low time reaction with this concentration because of the temperature and pressure unable to formation multi turns to lead the nanorods or nanotube structured this conclusion is agree with the XRD behavior(fig 3.3a) . The results is Appropriate with the granularity cumulating distribution (fig 3.15) and AFM images (fig 3.18 a).

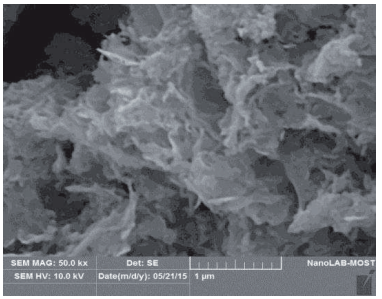

Fig 3.31 shows growth of the ZnO are prepared from 1g ZnO nanoparticles with 6M NaOH at 70 ^{o}C for 24 h appeared the lettuce leaf structure

The FE-SEM images ZnO nanotubes structure prepared from 1g ZnO nanoparticles with 6M NaOH at 70 ^{o}C for 48h are showing in figure 3.32.the outer diameters about 60-120nm and inner diameters about 20-90nm, the wall thickness are found about 10-60nm (fig 32c).This result also indicated that is high inner pressure with low outer pressure during the growth processer. The results are agreements with AFM report (fig 3.16 and fig 3.18 b) and XRD behavior (fig 3.3b).

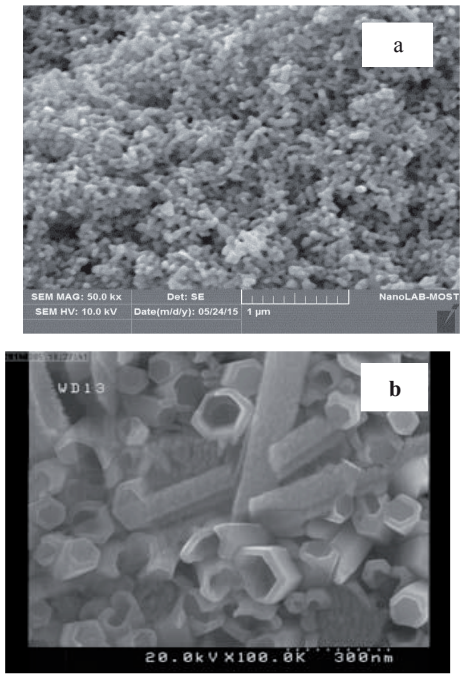

Fig 3.32: a and b shows growth of the ZnO are prepared from 1g ZnO nanoparticles with 6M NaOH at 70 ^{o}C appeared the nanotubes structure 48 h

Figure 3.33 show the FE-SEM images of ZnO nano sticks structure prepared from 1g ZnO nanoparticles with 6M NaOH at $70^{o}C$ for 72h.. It has been observed that the change of the reaction time and growth temperature contributes to a large variation on the morphology of nanostructures. The average diameters are found about 97 nm with lengths about 5-9µm. The FE-SEM images are agreement with AFM resulting (fig 3.17 and 3.18c) and XRD behavior (fig 3.3 c).

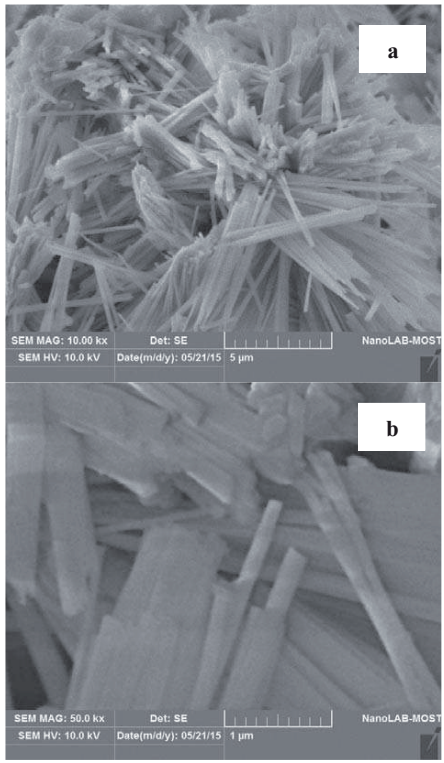

Fig 3.33:a and b shows growth of the ZnO are prepared from 1g ZnO nanoparticles with 6M NaOH at 70 ^{o}C for 72h appeared the nano sticks structures

3-3-2-4 Scan Electron Microscopic (SEM) and Field Emission Scan Electron Microscopic (FE-SEM)) for ZnO nanostructures-prepared with (6M) NaOH at 90

The FE-SEM over view image of ZnO nanostructures of 1 g ZnO nanoparticles and 3M of NaOH with different growth time 24, 48 and 72hour are shown in figures 3.34, 3.35 and 3.36 respectively at 90 ^{o}C.

It can be clearly seen the images from figure 3.34 (growth time reaction 24h) that the heterogeneous structures multilayers nano sheets

and nanoparticles it's clear that the average grain size about 82 nm with the nano scale for width the plates this result is comfortable and agreement with the AFM report (fig 3.20 and fig 3.23a) and agreement with the XRD behavior (fig 3.4a).the preparation parameters (concentration ,temperature, and reaction active time)ascribed to this conditions are not Enough to changes all nanoparticles to another structure because of the all growth formation secure at 24h.

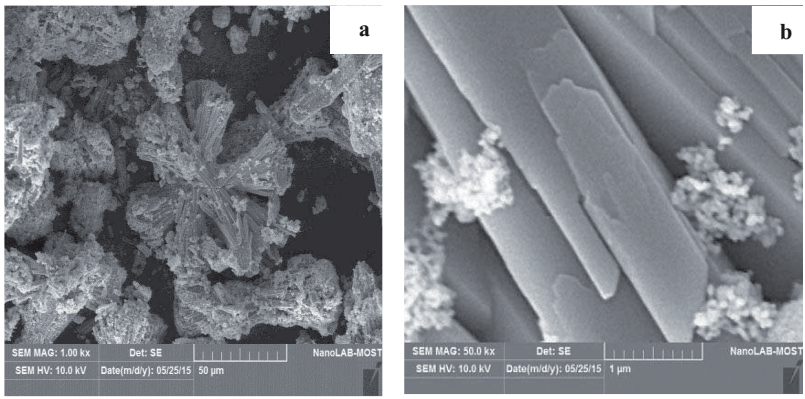

Fig 3.34 :a and b Shows growth of the ZnO are prepared from 1g ZnO nanoparticles with 6M NaOH at 90 ^{o}C for 24h appered hetrogeneous stracture (nanosheets and nanoparticles)

Figure 3.35 shows the images growth reaction time 48h it can be clearly seen from the nanorods structured of ZnO growth with average diameters about 86nm(45-120nm). The results are pointing to the inner pressure is less than outer pressure of structure grown for this process, it was indicated the agreement with the interpreted nanorods formation. During the growth process with the reaction parameters ZnO nuclei to assure the growth of nanorods have pressure cause temperature lead to inform this structure. The FE-SEM images are agreement with AFM report (fig 3.21 and 3.23b) and XRD behavior (fig 3.4 b).

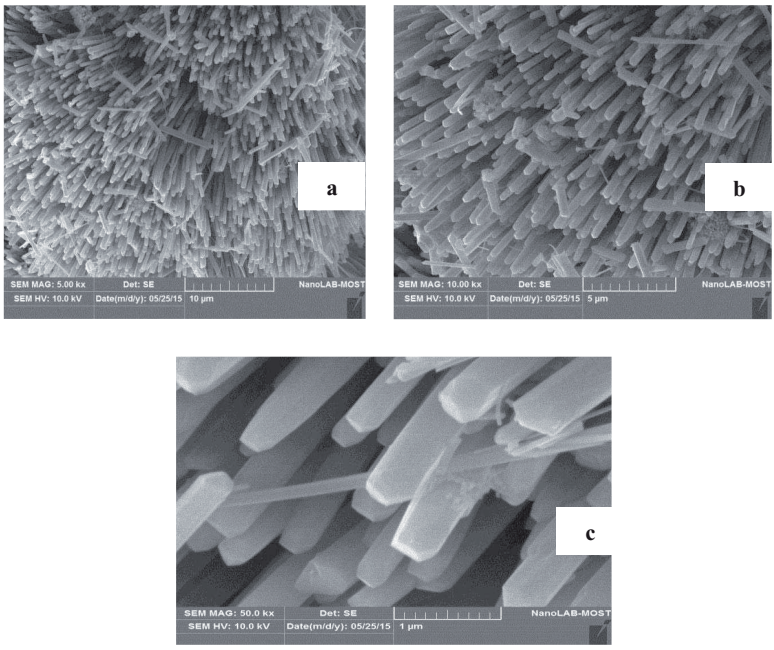

b

Fig 3.35 :a ,b and c shows growth (nanorods) of the ZnO are prepared from 1g ZnO nanoparticles with 6M NaOH at 90 ^{o}C for 48h

Figure 3.36 shows the images of ZnO structured preparation from 6M NaOH at 90 ^{o}C for 72h growth reaction time 72h it can be clearly seen non structures recognize description are founded .The growth process in accordance with these parameters (concentration, temperature, reaction time) produced forms cannot be described growth process in which , to the presence of randomly structures and that tests all of the X-ray and AFM reported compatible with the FE-SEM images

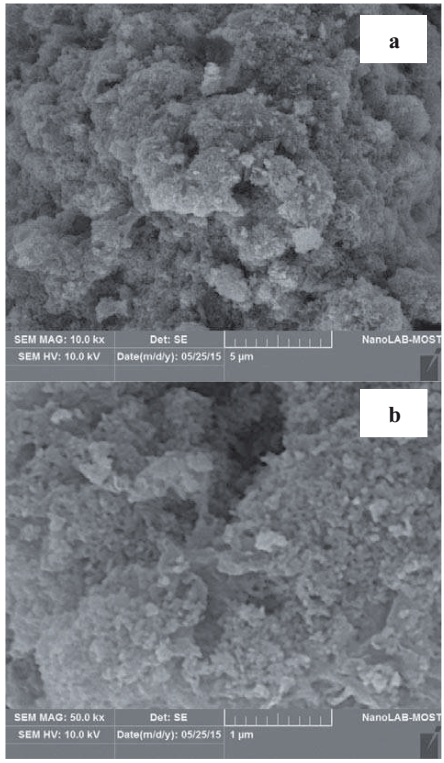

Fig 3.36:a and b shows non structures with 6M NaOH at 90 ^{o}C for 72h

Summary results obtained from the preparation for the production of nanoscale structures growth are summarized in the table 3.5

Table 3.5 The nano structures were obtained with all prepared conditions

NaOH conce.	Temp. ^{o}C	Reaction time(hour)	Higher dislocation density ($line^2/m^2$)	Lattice plane	Nano structure growth
3M	70	24	$3.51x10^{15}$	(101)	Heterogeneous structures(multilayers nanoplates +nanoparticles)
		48	$11.9x10^{15}$	(101)	Initially ZnO nanotubes
		72	$2.8x10^{15}$	(101)	nanotubes
3M	90	24	$1.5x10^{15}$	(110)	nanobelts
		48	$5.9x10^{15}$	(112)	nanorods
		72	$1.3x10^{15}$	(100)	flowerlike
6M	70	24	$4.89x10^{15}$	(101)	Lettuce leaf
		48	$4.171x10^{15}$	(101)	nanotubes
		72	$5.95x10^{15}$	(101)	nanosticks
6M	90	24	$1.01x10^{15}$	(101)	Heterogeneous structure(nanosheets+ nanoparticles)
		48	$2.89x10^{15}$	(101)	Nanorods
		72	$0.936x10^{15}$	(101)	Non structures recognize

3.4 *PL properties for ZnO prepared using different method:*

Photoluminescence (PL) studies provide information of different energy state available between valence and conduction bands responsible for irradiative recombination. These electron hole pairs (excitons) recombine within the crystal, sometimes at impurity sites as bound excitons if the semiconductor is extrinsically doped with impurities or

recombine at structural defect sites or intrinsic defects and this recombination causing emission of an optically measurable photon. PL measurements have been performed in order to evaluate the optical properties of the ZnO thick films prepared by different methods and conditions. Figure 3.37 shows the measured PL spectra for ZnO structures have nanotubes and nanorods prepared by hydrothermal method with the conditions were preparations. In this figure we are seen The PL intensity of ZnO nanotubes structure prepared with 3M (NaOH) at 70 ^{o}C for 72h consist of two peaks at 360nm and 390nm refer to direct of electron band, and weak emission of UV this result is agreement with the FE-SEM images and weak band UV emission. The another PL spectra for ZnO nanorods structure prepared with 3M (NaOH) at 90 ^{o}C for 48h appeared three peaks centered around 361nm, 388 nm and 485 nm respectively where the first peak refers to direct transition of electrons band to band, while the second band UV emission peak (388 nm) related to recombination's of free exciton sand the third is the green emission. The visible range emission of the ZnO can be attributed to radiative recombination through point defects in the ZnO lattice, such as oxygen vacancies, zinc vacancies, oxygen interstitials, zinc interstitials, [97].

The PL intensity of all peak positions of UV emission for the ZnO 386 nm are clear and high This suggests that the ZnO well crystalline with a wurtzite structure, while the green emission broadening refers to the defects in the film, all films green pecks have a shift towards blue shift indicating nanostructures, this agree with the XRD and SEM results.

The ZnO nanotubes structure were prepared with 6M (NaOH) at 70 ^{o}C for 48h it was PL intensity have three peaks centered around 362nm,392 nm and 481 nm respectively. The first peak refers to direct transition band to band, while the second band UV looks very week emission peak (381 nm), the third is due to the ionized oxygen vacancies

through the recombination of photon-generated hole and electron occupying oxygen vacancy. The PL intensity of all peak positions of UV emission for the ZnO 389 nm This suggests that the ZnO well crystalline with a wurtzite structure, while the green emission broadening refers to the defects in the film, all so the films green pecks have a shift towards blue shift indicating nanostructures, this agree with the XRD and SEM results. While the PL spectra for ZnO nanorods structure prepared with 6M (NaOH) at 90 ^{o}C for 48h have three peaks centered around 356,389 nm and 476 nm respectively. Corresponding to band to band, near band energy (NBE), and green luminous (GL) respectively. The PL intensity of peak positions of UV emission for the ZnO 389 nm is high and narrow this indicating that the ZnO well crystalline with a wurtzite structure, while the green emission broadening refers to the defects in the film, all so the films green pecks have a shift towards blue shift indicating nanostructures, this agree with the XRD and SEM results.

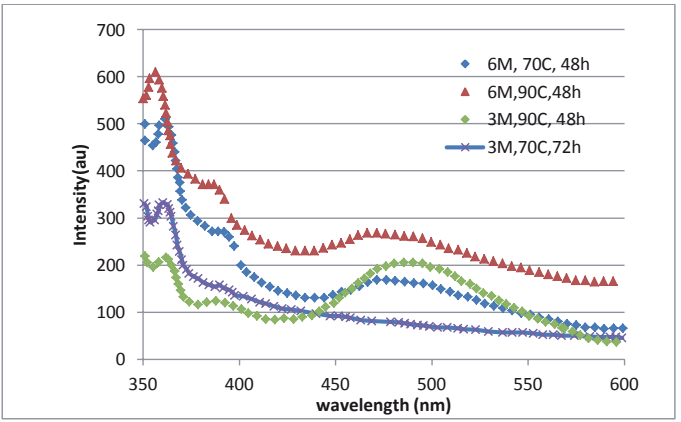

Figure 3.37: PL for ZnO nanotubes and nanorods prepared by hydrothermal method with different conditions

The values of energies estimated from PL at different wavelengths are reported on the table 3.6(suing eq. 1.1).

Table 3.6: Values of energies estimated from PL at different wavelengths

Preparation Condition	*E_1 (eV)*	*E_2 (eV)*	*E_3 (eV)*
3M(NaOH),70 ^{o}C,72h	*3.44 at 360nm*	*3.17-390nm*	*-*
3M(NaOH),90 ^{o}C 48h	*3.43 at 361nm*	*3.21 at 388nm*	*2.56 at 485nm*
6M(NaOH),70 ^{o}C,48h	*3.43 at 362nm*	*3.16 at 392nm*	*2.54 at 488nm*
6M(NaOH),90 ^{o}C,48h	*3.48 at 356 nm*	*3.19 at 389nm*	*2.61 at 476nm*

CHAPTER FOUR

CONCLUSIONS AND FUTURISTIC IDEAS

4.1 Conclusions

According to results presented in this work it was conclude the following points:

1. The device locally manufacturing (homemade) of hydrothermal method, for synthesis of nanostructure materials is restricted only up to 90 ^{o}C, therefore the device must be development of the design to exceed the heat degrees were used .
2. The hydrothermal method used is suitable efficiently ZnO nanostructures especially for nanotubes and nanorods.
3. All the prepared films are polycrystalline in nature but only the nanotubes and nanorods have wurtzite hexagonal structure while the other structures were varying grown wurtzite hexagonal structure because of the prepared conditions (concentration, temperature, pressure, and reaction time) are not adequacy to achieve the required structure, The highest surface roughness and peak to peak roughness is indicated to optimization preparation of nanostructures.
4- The grown direction for hydrothermal method shows preferring direction for nanotubes and nanorods to be majoring strong growth especially toward lattice planes (101), (100), and (002).
5- The shape and structure of the product depends strongly on the preparation conditions.

6-The PL properties of ZnO nanostructures were strongly dependent on NaOH concentration and dislocation density of the growth.

4.2 Futuristic Ideas

The interesting result obtained in this work impel us to offer some to suggest for the development of future studies on syntheses and

enhancement of ZnO nanostructure application such as gas sensor and solar cells.

1- Design a new device or development the preparation system to use for high temperature exceeds 150 ^{o}C.
2- Preparation another nanostructure materials with different conditions.
3- Study the effect of annealing temperature on the properties of ZnO nanostructures prepared by hydrothermal method.
4- Study the effect of changing the surfactant agent on the structural and of the prepared ZnO nanostructures by hydrothermal method.
5- Synthesis of ZnO nanostructures with other methods such as simple evaporation and chemical method.
6- Study the effective of additive material to ZnO nanostructure on optical and electrical properties.
7- Fabrication nanomaterials for chemical sensing with different preparation and study the preparation conditions effects on sensing parameters (sensitivity, selectivity and stability).
8- Study the possibility working from the ZnO nanostructure product to fabrication solar cells effect of annealing temperature on the properties of ZnO prepared by hydrothermal method.

References

[1] T. Steiner,"**Semiconductor Nanostructures for Optoelectronic Applications**"© artech house, inc., (2004).

[2] Z. Yang, Y. Huang, G. Chena, Z. Guo, Sh. Cheng, Sh. Huange, "**Ethanol gas sensor based on Al-doped ZnO nanomaterial with many gas diffusing channels**" Sensors and Actuators,B 140 549-556,(2009).

[3] K. V. Gurav, U. M. Patil, S.W. Shin, S.M. Pawar, J. H. Kim, C.D. Lokhande, "**Morphology evolution of ZnO thin films from aqueous solutions and their application to liquefied petroleum gas (LPG) sensor**", Journal of Alloys and Compounds, 525, 1-7, (2012).

[4] L. Tillstra, S. brougton, R. Tanke Daniel Jelski, V. French, G. Zhang, K. Popov, B. Western and Th.George, "**The science of nanotechnology an introductory text**" Nova Science Publishers, Inc. New York, (2008).

[5] A. Talbi, F. Sarry, M. Elhakiki, L. Le Brizoual, O. Elmazria, P. Nicolay, P. Alnot, "**ZnO/quartz structure potentiality for surface acoustic wave pressure sensor**" Sensors and Actuators A 128,78-83(2006).

[6] I. Victor Klimov, "**semiconductor and metal Nanocrystals Synthesis and electronic and optical properties**", Copyright (2004), by Marcel Dekker, Inc.

[7] D. Dhawale, C. Lokhande, "**Chemical route to synthesis of mesoporous ZnO thin films and their liquefied petroleum gas sensor performance**" Journal of Alloys and Compounds 509, 10092-10097, (2011).

[8] H.Tang, M. Yan, Hui Zhang, Li Shenzhong, Xingfa Ma, M. Wang, D. Yang, " **A selective NH_3 gas sensor based on Fe_2O_3-ZnO nanocomposites at room temperature**" Sensors and Actuators 114.910-915,(2006).

[9] J. Haeng, G. Choi, "**Selective Co gas detection of CuO- and ZnO – doped SnO_2 gas sensor**", sensor and Actuators 75 , 56-61,(2001).

[10] M. Chougule, Sh. Sen, V.B. Patil, "**Fabrication of nanostructured ZnO thin film sensor for NO monitoring**" Ceramics International 38, no.4 , 2685,(2012).

[11] Y. Jaeseok, J. Min Lee, W.Park, "**Vertically aligned ZnO nanorods and graphene hybrid architectures for high-sensitive flexible gas sensors**" Sensors and Actuators vol. 155, pp.264-269(2011).

[12] S. Bangale, S. Bamane, "**Preparation and Study of H_2S gas sensing behavior of $ZnFe_2O_4$ thick film resistors**", Sensors and Transducers Vol. 137, 123-136, (2012).

[13] Y. Hu, X. Zhou, Q. Han, Q. Cao, Y. Huang, "**Sensing properties of CuO/ZnO heterojunction gas sensors**", Materials Science and Engineering vol.99, pp.41-43,(2003).
[14] H. Chen, Y. Liu, Ch. Xie ,Jun Wu, D. Zeng, Yichuan Liao, "**A comparative study on UV light activated porous TiO_2 and ZnO film sensors for gas sensing at room temperature**", Ceramics International ,vol.38, pp.503-509 ,(2012).
[15] Sh. Xu, Z. Wang, "**One-Dimensional ZnO Nanostructures: Solution Growth and Functional Properties**", Nano Res., 3(9): 676-684,(2010).
[16] H. Chen, Y. Liu, Ch. Xie, J. Wu, D. Zeng, Yichuan Liao, "**A comparative study on UV light activated porous TiO2 and ZnO film sensors for gas sensing at room temperature**", Ceramics International ,vol.38 , pp.503-509,(2012).
[17] Ch. Jin, S. Park, H. Kim, Ch. Lee, "**Ultrasensitive multiple networked Ga2O3-core/ZnO-shell nanorod gas sensors**", Sensors and Actuators vol. 161,pp. 223-228 ,(2012).
[18] K.Kim, H-R Kim, "**Design of Highly Sensitive C2H5OH Sensors Using Self-Assembled ZnO Nanostructures**", Sensors, 11, pp.9685-9699, (2011).
[19] Ch. Poole, Jr. Owens, "**Introduction To Nanotechnology**", Copyright Q, by John Wiley and Sons, Inc,(2003).
[20] C. Br´ echignac P. Houdy M. Lahmani (Eds.) "**Nanomaterials and Nanochemistry**", Springer-Verlag Berlin Heidelberg (2007).
[21] A. Aslani, "**Microscopy Methods in Nanochemistry**", Current Microscopy Contributions to Advances in Science and Technology, (2012).
[22] M.-P. Pileni, "**Nanocrystals Forming Mesoscopic Structures**", Copyright WILEY-VCH Verlag GmbH and Co. KGaA, Weinheim, (2005).
[23] A. Zunger, "**Electronic-Structure, Theory of Semiconductor Quantum Dots**", MRS Bulletin,vol. 23, pp 35-42 (1998).
[24] J. David Lockwood, "**Nanoelectronics and Photonics**", National Research Council of Canada, (2008).
[25] J. Mark Jackson "**Microfabrication and Nanomanufacturing"**, Edited by ©, by Taylor and Francis Group, LLC,(2006).
[26] É. Knystautas, **Engineering Thin Films and Nanostructures with Ion Beams**, ©, by Taylor and Francis Group, LLC,(2005).
[27] N. H. Al-Hardan, M. J. Abdullah, A. Abdul Aziz, "**Sensing mechanism of hydrogen gas sRF-sputtered ZnO thin films**", international journal of hydrogen energy,vol. 35, pp.4428–4434,(2010).
[28] A. La Rosa, M. Yan, R. Fernandez, X. Wang and E. Zegarra, "**Top-down and Bottom-up approaches to nanotechnology An overview in**

the context of developing", Portland State University, Portland, Oregon 97207, USA, (2011).
[29] Z.Wang, "**Zinc oxide nanostructures: growth, properties and Applications**", J. Phys.: Condens. vol 16, pp.R829-R858, (2004).
[30] C. N. R. Rao, A. Müller and A. K. Cheetham (Eds.), "The Chemistry of Nanomaterials, Synthesis", Properties and Applications in 2 Volumes, Wiley-VCH Verlag GmbH and Co. KGaA. (2009).
[31] Ji-Guang Li, Takamasa Ishigaki, and Xudong Sun, "Anatase, Brookite, and Rutile Nanocrystals via Redox Reactions under Mild Hydrothermal Conditions: Phase-Selective Synthesis and Physicochemical Properties", J. Phys. Chem. C, 111(13), 4969 (2007).
[32] J. Lee, M. Orilall, S. Warren, M. Kamperman, F. DiSalvo and U.Wiesner. "Direct access to thermally stable and highly crystalline mesoporous transition-metal oxides with uniform pores", Nature Mater. 7, 222-228 (2008).

[33] Z. Fan and Jia G. Lu, "**Zinc Oxide Nanostructures: Synthesis and Properties**", Journal of Nanosince and nanotechnology, (2005).

[34] V. A. Coleman, C. Jagadish, "**Basic Properties and Applications of ZnO**",Science Direct P.P 1-20 (2006).
[35] J. Wan, X. Yan, J. Ding, M. Wang, K. Hu, "Self-organized highly ordered ZnO nanotubes in organic aqueous system", Materials Characterization, Vol. 60 , No. 12 , 1534-1540, (2009).
[36] Dong-Seok Seo, Jong-Kook Lee, and Hwan Kim, "Preparation of nanotube-shaped ZnO powder", Journal of Crystal Growth, Vol. 229, Issues 1–4, P. 428, (2001).
[37] C. C. Koch, "**Top-Down synthesis of nanostructured materials: mechanical and thermal processing methods**", Rev. Adv. Mater. Sci. 5, 91-99(2003).
[38] J. Behari "**Principles of nanoscience: An overview**", Indian Journal of Experimental Biology, Vol.48, pp1008-1019, (2010).
[39] B. Kear, G. Skandan, **Nanostructured Materials**, , Wiley-VCH Verlag GmbH and Co. KGaA, Weinheim (2005).
[40] L. Fillipponi, Duncan Sutherland, "**Fundamental Concept in Nanoscince and Nanotechnology**", Aarhus University, Denmark, (2010).
[41] FLiu, PJCao, HRZhang, JQLi, H J Gao, "**Controlled Self-Assembled Nanoaeroplanes, Nanocombs, and Tetrapod-Like Networks of Zinc Oxide**", Nanotechnology 15, 949-952(2004).
[42] J. Z. Liu, P. X. Yan, G. H. Yue, J. B. Chang, R. F. Zhuo, D. M. Qu, "**Controllable synthesis of undoped/Cd-doped ZnO nanostructures**", Materials Letters 60, 3122-3125(2006).

[43] L. Li, “Functional Photo-electrochemical Devices for Solar Cells and Solar Fuels Based on Molecular Components”, Doctoral Thesis, Stockholm, pp. 4-6, (2012).
[44] J. T. Jiu, S. Isoda, F. M. Wang and M. Adachi, “Dye-sensitized solar cells based on a single crystalline ZnO nanorod film”, J. Phys. Chem. B, 110 (5), p. 2087, (2006).
[45] A. Kołodziejczak-Radzimska, T.Jesionowski, "**Zinc Oxide-From Synthesis to Application",** A Review, Materials, 7, 2833-2881, (2014).
[46] Y. Zhaoy, Y.Kwon, "**Templateless Hydrothermal Synthesis of Aligned ZnO Nanorods**", Chemistry Letters Vol.33, No.12, 1578-1579(2004).
[47] T. Mousavand, M. Umetsu, S. Takami, T. Adschiri, "**Hydrothermal Synthesis of Fine Zinc Oxide Nano-Particles under Supercritical Conditions**", Institute of Multidisciplinary Research for Advanced Materials, Tohoku University,14th international conference on the properties of water and steam in Kyoto(2010).
[48] Z. Zheng, "**Synthesis and Modifications of Metal Oxide Nanostructures and Their Applications**", thesis Queensland University of Technology, (2009).
[49] K. M. Anisur Rahman, Susan C. Schneider and Martin A. Seitz, J. .Am, Ceram.Soc. 80 (5), 1198-1202 (1997).
[50] K. Kim, Hae-Ryong Kim, Kwon-Il Choi, Hyo-Joong Kim, Jong-Heun Lee, "**Design of Highly Sensitive C_2H_5OH Sensors Using Self-Assembled ZnO Nanostructures**", Sensors, 11, 9685-9699(2011).
[51] A. Adnan Hateef, B. Daram Balawa, A. Salehm, M. Wailed Mahmmod, "**Effect of the thickness on electrical properties of TiO_2 thin films, prepared by thermal chemical spray pyrolysis deposition**", International Research Journal of Engineering Science, Technology and Innovation ,Vol. 1, No. 6,PP.175-179, (2012).
[52] M. Ratner, D. Ratner, "**Nanotechnology: A Gentle Introduction to the Next Big Idea**", About Prentice Hall Professional Technical Reference, p.208, (2002).
[53] M. Shah1, Kh. S. Karimov, Zubair Ahmad1, M. H. Sayyad, "**Electrical Characteristics of Al/CNT/NiPc/PEPC/Ag Surface-Type Cell**", chin. Phys. lett. Vol. 27, No. 10, 106102(2010).
[54] P. S. Kireev, "**Semiconductors Physics**", Translated from Russian by M.Samokhvalov, MIR Puplishers, Moscow (1978).
[55] Deng, Y. Nan, C. W. Wei, G. D. Guo, L. Lin, Y. H**.”Organic-assisted growth of bismuth telluride nanocrystals**” Chem, Phys. Lett., 374, 410-415(2003).
[56] Lu, Q. Gao, F. Komarneni, S. AdV. Mater, 16, 1629-1632(2004).

[57] J. L. Lock, N. Sun, T. Christensen, M. Søndergaard, M. Hald, P. Hng, H. H. Ma, J. Iversen, B. B. ACS Nano, 4, 2523-2530, (2010).

[58] Shou-Yi Kuo, "**Introduction to Photoluminescence Spectroscopy**", Chang Gung University copyright (2004).
[59] T. Gfroerer, "**Photoluminescence in Analysis of Surfaces and Interfaces**", JohnWiley & Sons Ltd, Chichester, (2000).
[60] Z. Zou, Changsheng Xie, Shasha Zhang, Chaoqun Yang, Guozhu Zhang, Li Yang, "**CdS/ZnO Nanocomposite Flm and its Enhanced Photoelectric Response to UV and Visible Lights at Low Bias**", Sensors and actuators B 188, 1158-1166, (2013).
[61] V.A. Stoica, "**Optical Characterization of Compound Semiconductors Using Photoconductivity and Photoreflectance**", Thesis of Master, Morgantown, West Virginia, (2000).
[62] S. P. Chang, S. J. Chang , Y. Z. Chiou, C. Y. Lu, T. K. Lin , Y. C. Lin, C. F. Kuo, H. M. Chang, **ZnO Photoconductive Sensors Epitaxially Grown on Sapphire Substrates**", Sensors and Actuators A 140, 60-64, (2007).
[63] K. Saravanakumar, "**Structural, Optical and Photoconductivity Studies of ZnO: As Nanocrystalline Thin Films**", Contemporary Engineering Sciences, Vol. 4, No. 3, 101-117, (2011).
[64] C.C. Tsai and H. Teng, "Structure features of nanotubes synthesized from NaOH treatment on TiO_2 with different post-treatment", Chem. Mater. 18, 367 (2006).

[65] A. Robinson, "**Scientific Needs for Future X-Ray Sources in the U.S.**", Lawrence Berkeley National Laboratory University of California Berkeley, CA 94720, (2008).
[66] T. Radeti, "**Fundamentals of Scanning Electron Microscopy and Energy Dispersive X-ray Analysis in SEM and TEM**", NFMC Spring School on Electron Microscopy, April, (2011).
[67] Y.Q. Wang, G.Q. Hu, X.F. Duan, H.L. Sun and Q.K. Xue, "Microstructure and formation mechanism of ZnO nanotubes", Chemical Physics Letters, Vol. 365, Issues 5–6, pp. 427–431, (2002).
[68] T. Sato, Sue K., Tsumatori H., Suzuki M., Tanaka S., Kawai-Nakamura A., Saitoh K., Aida K., Hiaki T. J., **"Thermal And Structural Analysis For A Reactor Used In Hydrothermal Synthesis Under Supercritical Condition"** ,Supercrit. Fluids,**,** 46, 173-177, (2008)

[69] D. Ravnsbæk, Filinchuk Y., Cerenius Y., Jakobsen H. J., Besenbacher F., Skibsted J. Jensen, **"Crystal chemistry of light metal borohydrides**" Angew. Chem. Int. Ed, 48, 6659-6663, (2009).

[70]V. Reverchon, Adami R. J.,"**Nanomaterials And Supercritical Fluids"** Supercrit. Fluids, 37, 1-22, (2006).

[71] M. Jensen H., Bremholm, Nielsen R. P., Joensen K. D., Pedersen B. H., Chen Y.-S., Almer J., Søgaard E. G., Iversen S. B., Iversen B. B. Angew,"**Understanding the Formation and Evolution of Ceria Nanoparticles Under Hydrothermal Conditions"** Chem. Int. Ed**,** 46, 1113-1116(2007).

[72] *X.-F. Shen, Ding Y.-S., Hanson J. C., Aindow M., Suib, S. L. J.,* ***"Nonthermal synthesis of three-dimensional metal oxide structures under continuous-flow conditions and their catalytic applications"*** *Am. Chem. Soc. 128, 4570-4571 (2006).*

[73] C.Tyrsted, Becker J., Hald P., Bremholm M., Pedersen J., Chevallier J., Cerenius Y., Iversen S. B., Iversen, B. B., "Quantifying the Nucleation and Growth Kinetics of Microwave Nanochemistry Enabled by in Situ High-Energy X-ray Scattering" Chem. Mater,
doi:10.1021/cm903316s(2010).

[74] C. Aymonier, Loppinet-Serani A., Revero´ n H., Garrabos Y., Cansell F. J.,"**Tuning Al_2O_3 Crystallinity Under Supercritical Fluid Condition:effect on sinering**", Supercrit. Fluids, 38, 242-251, (2006).

[75] M. M. Woolfson., "**An Introduction to X-ray Crystallography**", 2nd ed. Cambridge University Press, (1997).

[76] Ikram Ul Haqand Abdul-Majeed Azad, **"Experimental Artifacts for Morphological Tweaking of Chemical Sensor Materials: Studies on ZnO**", Sensors, 12, 8259-8277 (2012).
[77] Qu Zhou, Weigen Chen, Lingna Xu, Shudi Peng, "**Hydrothermal Synthesis of Various Hierarchical ZnO Nanostructures and Their Methane Sensing Properties**", Sensors, 13, 6171-6182(2013).
[78] F. Guo, Bin Yang, Yongbo Yuan, Zhengguo Xiao, Qingfeng Dong, Yu Bi, Jinsong Huang, "**A Nanocomposite Ultraviolet Photodetector Based on Interfacial Trap-Controlled Charge Injection**", nature nanotechnology, 10/1038/NNANO.87(2012).

[79] M. Yezhelyev, Yacoub, R., O'Regan R., **"InorganicNanoparticles For Predictive Oncology Of Breast Cancer"** Nanomedicine, 4, 83-103, (2009).

[80] C. Aymonier, Loppinet-Serani A., Revero´ n H., Garrabos Y., Cansell F. J.,"**Tuning Al_2O_3 Crystallinity Under Supercritical Fluid Condition:effect on sinering**", Supercrit. Fluids, 38, 242-251, (2006).

[81]Y. Zhao, Young-Uk Kwon, "**Templateless Hydrothermal Synthesis of Aligned ZnO Nanorods**", Chemistry Letters Vol.33, No.12 (2004).

[82]Yong-hong Ni, Xian-wen Wei, Jian-ming Hong, "**Hydrothermal preparation and optical properties of ZnO nanorods**", Materials Science and Engineering B 121, 42-47(2005).

[83] J.Z. Liu, P.X. Yan, G.H. Yue, J.B. Chang, R.F. Zhuo, D.M. Qu," ***Controllable synthesis of undoped/Cd-doped ZnO nanostructures***", Materials Letters 60 3122–3125(2006).

[84] O. Lupan, Guangyu Chai, Lee Chow, "**Novel hydrogen Gas Sensor Based on Single ZnO Nanorod**", Microelectronic Engineering 85, 2220-2225(2008).

[85]R. Yousefi, B. Kamaluddin, M. Kavosh, "**Fabrication and Characterization of ZnO Nanowires and Nanodiscs Grown in Modified Thermal Evaporation Set-Up**", Iranian Physical Journal, 3-2, 29-32, (2009).

[86] M.-W. Ahn, K.-S. Park, J.-H. Heo, D.-W. Kim, K.J. Choi, J.-G. Park, "***On-chip fabrication of ZnO-nanowire gas sensor with high gas sensitivity***", Sensors and Actuators B 138 168–173(2009).

[87] H. Lv, D. D. Sang, H. D. Li, X. B. Du, D. M. Li, G. T. Zou, "***Thermal Evaporation Synthesis and Properties of ZnO Nano/Microstructures Using Carbon Group Elements as the Reducing Agents***", Nanoscale Res Lett 5, 620–624, (2010).

[88] Kang-Min Kim, Hae-Ryong Kim, Kwon-Il Choi, Hyo-Joong Kim, Jong-Heun Lee, "**ZnO Hierarchical Nanostructures Grown at Room Temperature and Their C_2H_5OH Sensor Applications**", Sensors and Actuators B155, 745-751 (2011)..

[89] Shao-Lin Zhang, Jeong-Ok Lim, Jeung-Soo Huh, Jin-Seo Noh, Wooyoung Lee, "**Two-Step Fabrication of ZnO Nanosheets for High-Performance VOCs Gas Sensor**", Current Applied Physics vol. 13, pp. S156-S16, (2013).

[90] Jian-Fu Tang, Hsiu-Hsien Su, Yang-Ming Lub, Sheng-Yuan Chu, "**Controlled Growth of ZnO Nanoflowers on Nanowall and Nanorod Networks Via Hydrothermal Method**", ARTICLE TYPE**,** CrystEngComm, DOI: 10.1039/C4CE01940G**, (**2014).

[91] A.A Thamir.hassan **"*Enhancement of gas response of annealed ZnO film for hydrogen detection***" Iraqi journal of physics,40112,No.23,PP.73-79(2014) .

[92] H. Chen, Yanyan Fang, Senlin Li, Zhiqiang Qi, Xuhua Huang, Yu Tian, "**Synthesis of ZnO Nanowire Array Film on Mg-Doped Gallium Nitride Substrate by Simple Hydrothermal Method**", Synthesis and Reactivity in Inorganic, Metal-Organic, and Nano-Metal Chemistry, 45, 1045-1048(2015).
[93] Ikram Ul Haqand Abdul-Majeed Azad, **"Experimental Artifacts for Morphological Tweaking of Chemical Sensor Materials: Studies on ZnO"**, Sensors, 12, 8259-8277 (2012).
[94] F. Guo, Bin Yang, Yongbo Yuan, Zhengguo Xiao, Qingfeng Dong, Yu Bi, Jinsong Huang, "**A Nanocomposite Ultraviolet Photodetector Based on Interfacial Trap-Controlled Charge Injection**", nature nanotechnology, 10/1038/NNANO.87(2012).
[95] J. Committee on powder Diffraction Standard, Powder Diffraction file No.36-1451

[96] A.A Thamir Hassan,M.abdilkareem Ali and Ali Qassim "**Nanoroods and flowerlike by hydrothermal growth method without catalsts**" The 5th International Scientific Conference on nanotechnology and advanced materials and their applications ICNAMA 3-4 Nov,Vol.33,PB,No.6,2015.

[97] J. I. Pankove, "***Optical Processes in Semiconductors***", Prentice–Hall, Inc., Englewoodcliffs, New Jersy (1971).

الخلاصه

تم تحضير التركيبات النانوية لأوكسيد الخارصين بطريقة الهدرجة الحرارية ,ان هذه التقنية تتميز بخصائص مهمة منها انها رخيصة الثمن ولا تتطلب طاقة عالية مع سهولة التحضير وبيئة عمل آمنة.

غرام واحد من حبيبات اوكسيد الخارصين يتم وضعها مع محلول هيدروكسيد الصوديوم وبتراكيز 3,6 مولارتي لتكون المادة الاساسية للتفاعل الكيميائي ويتم خلطها من خلال محرك مغناطيسي للتجانس .المحلول يوضع داخل البوتقة وتحكم اغلاقها وبدرجات 70 و90 درجة مئوية وبشكل منفصل لفترات زمنية 24,48,72 ساعة .لوحظ خلال التركيز 10 مولارتي لم يتكون أي تبلور خلال هذه الفترات الزمنية ولذلك استبعدت من دراسة الخواص النتائج من هذه الرسالة.

تم تحضير تركيبات نانوية بنجاح للتركيزين3,6 مولارتي بطريقة الهدرجة الحرارية اعلاه حيث تم الحصول على تركيبات نانوية مختلفة (انابيب , قضيبات ,احزمة, عصيات, تراكيب ورقية تشبه اوراق الخس, وتراكيب زهرية, وتراكيب متراكبة)

درست تأثير عمليات التحضير على السطح وعملية التبلور وخصائص التركيبات من خلال حيود الاشعة السينية والمجهر الالكتروني الماسح –تأثير المجال. ان جميع النماذج المفحوصة بالأشعة السينية اظهرت شكل سداسي نوع Wurtzite وكثافة انخلاعات عالية لكل التراكيب النانوية بأتجاه المستوي (101) ماعدا في حالة التراكيب المحضرة بتركيز 3M NaOH وبدرجة حرارة 90 درجة مئوية ولكل الزمان.

صور المجهر الالكتروني الماسح –تأثير المجال بينت تركيب انابيب اوكسيد الخارصين بظروف (3مولارتي,70درجة مئوية,72 ساعة)و (6مولارتي,70درجة مئوية,48 ساعة) , قضيبات نانوية (3مولارتي,90 درجة مئوية,48 ساعة) و(6 مولارتي,90درجة مئوية, 48 ساعة) , تركيبات زهرية(3 مولارتي,90 درجة مئوية ,72 ساعة) ,تركيبات اوراق الخس (6 مولارتي,70درجة مئوية,72 ساعة) , اعواد نانوية(6 مولارتي,70درجة مئوية,72 ساعة), تركيبات غير متجانسة (3 مولارتي,70درجة مئوية ,24 ساعة),

جسيمات نانوية والواح نانوية (6مولارتي,90درجة مئوية,24 ساعة), جسيمات نانوية وصفائح نانوية حيث لا يمكن ملاحظة تركيب بلوري مميز بظروف(6 مولارتي,90درجة مئوية ,72 ساعة). ان غشاء التركيبات النانوية المحضرة درست من خلال فحوصات المكروسكوب القوة الذرية وبينت خشونة عالية للظروف (72ساعة,3مولارتي,70درجة مئوية) و(48ساعة,3مولارتي,90درجة مئوية) و(6 مولارتي ,70درجة مئوية ,48ساعة)و (6مولارتي ,90درجة مئوية,48 ساعة). اظهرت قياسات الانبعاث الضوئي (PL) لأوكسيد الزنك النانوي والاعواد النانوية التركيب ازاحة نحو الطول الموجي الازرق مما يعني تزايد في فجوة الطاقة للتركيب النانوي الذي تم الحصول عليه.